Inter-Comparison and Validation of the FY-3A/MERSI LAI Product Over Mainland China

Lin Zhu, Jing M. Chen, Shihao Tang, Guicai Li, and Zhaodi Guo

***Abstract*—Leaf area index (LAI) is a key surface parameter that describes the structure of vegetation and plays an important role in Earth system process modeling. In this paper, a new set of LAI products (MERSI GLOBCARBON LAI) has been developed based on the GLOBCARBON LAI algorithm and one year of FY-3A/MERSI land surface reflectance data. MERSI GLOBCARBON LAI has been inter-compared and validated over mainland China against MODIS land surface reflectance (LSR) derived LAI (using the same algorithm) and field LAI measurements. MERSI GLOBCARBON LAI and MODIS GLOBCARBON LAI show continuous and smooth LAI distributions at the start and end of the growing season. For most areas in China, the two LAI products agree well. The temporal variation in MERSI GLOBCARBON LAI and MODIS GLOBCARBON LAI consistently follows the growing season. The largest LAI difference occurs during July, when MERSI shows a much higher frequency of retrievals than does MODIS. Through validation of LAI retrievals with field measurements, our study demonstrates that LAI derived from MERSI and MODIS land surface reflectance products have comparable accuracy. MODIS top-of-atmosphere simple ratio (MODIS TOA SR) is related to MERSI TOA SR with linear correlation coefficients greater than 0.6. After atmospheric correction, the correlation coefficient increases from 0.69 to 0.75 over cropland and from 0.82 to 0.93 over grassland. However, atmospheric correction can still give rise to substantial differences in the reflectance data between the two sensors. Furthermore, different land cover types and different terrain relief have contrasting influences on the atmospheric correction, and these influences reduce the agreement between the two LAI products. This study shows the great potential of FY-3A/MERSI data for global LAI retrieval.**

***Index Terms*—FY-3A/MERSI, GLOBCARBON, leaf area index, TERRA/MODIS.**

I. Introduction

REGIONAL and global water and carbon exchange between the land surface and the atmosphere depend greatly on the functioning of plant leaves [1]–[5]. Leaf area index (LAI), defined as half the total leaf area per unit ground surface area [6], is a key vegetation structural parameter of the Earth system used to quantify photosynthesis, respiration, evapotranspiration, canopy interception, energy exchange, and other ecohydrological processes [7]–[9].

Remote sensors with moderate resolution (pixel sizes from 250 m to several kilometers) provide daily and seasonal data at regional and global scales, and these may currently be the best tool to monitor spatial and temporal variations in LAI [10], [11]. Global LAI products have been derived from many remote sensing data sets such as NOAA/AVHRR, TERRA-AQUA/MODIS and SPOT/VEGETATION [12]–[15]. These data sets have provided unprecedented opportunities for studying the Earth's climate [3]. The development of China's new generation of polar-orbiting meteorological satellite series (FY-3) has greatly enhanced surface monitoring [16]. MERSI (Medium Resolution Spectral Imager) is a key multispectral instrument onboard FY-3 satellite [18]. The first two satellites in the series, the morning FY-3A (launched on 27 May 2008) and the afternoon FY-3B (launched on 5 November 2010) provide a 6-hourly revisit capability. This offers the prospect of new, more detailed global LAI products based on this data source. Recently, FY-3A/MERSI LAI Version 1 (MERSI GLOBCARBON LAI), an FY-3A test product from the National Satellite Meteorological Center of China (NSMC), was developed using the GLOBCARBON LAI algorithm [10], [14], [3] and one year of FY-3A/MERSI data. As many other global LAI maps are regularly produced, the accuracy assessment and validation of FY-3A/MERSI LAI are of key importance for potential users.

The overall quality of LAI products depends on several key factors that influence the accuracy of the final retrievals [4]. Uncertainty in input surface reflectance is one of the most important error sources [19], [4], [20]. Surface reflectance time series measured from spaceborne instruments, such as MOderate Resolution Imaging Spectroradiometer (MODIS), show apparent high-frequency noise that limits their information content [21]. The accuracy of surface reflectance products is most affected by the retrieval accuracy of aerosol optical thickness, the Lambertian surface approximation, topography, and viewing-illumination geometry effects [20], [11], [22], [21]. Although different land surface reflectance (LSR) products, such as MODIS surface reflectance collection C5 [23], VGT [24], and MERSI [17], all reduce the uncertainty in the atmospheric correction process using different approaches, the remaining uncertainty may still be considerable. Therefore, as the first step in validating and assessing the FY-3A/MERSI global product, it is desirable to compare the spatial performance of MERSI LSR and MODIS LSR products for LAI retrieval and to evaluate the consistency of LAI time series from different LSR products.

Manuscript received November 18, 2012; revised February 28, 2013; accepted August 19, 2013. This work was supported by the National Basic Research Program of China (Grant 2010CB950700), and China's Research and Development Special Fund for Public Welfare Industry (Meteorology GYHY200906022-1 and Meteorology GYHY200906029). *(Corresponding author: L. Zhu.)*

L. Zhu, S. Tang, G. Li, and Z. Guo are with the National Satellite Meteorological Center of China Meteorological Administration, Beijing, China (e-mail: zhulin@cma.gov.cn; tangsh@cma.gov.cn; ligc@cma.gov.cn; guozd@cma.gov.cn).

J. M. Chen is with the Department of Geography, University of Toronto, Toronto, Ontario, Canada (e-mail: chenj@geog.utoronto.ca).

Color versions of one or more of the figures in this paper are available online at http://ieeexplore.ieee.org.

Digital Object Identifier 10.1109/JSTARS.2013.2280466

The second source of uncertainty arises from misclassifications in the land cover map. Mixed pixel effects can further contribute to errors in land cover classification and introduce extra scaling bias, particularly in moderate-resolution remote sensing data [25], [26]. Pisek and Chen [4] demonstrated that differences in land cover classification for low-resolution images can lead to a difference of $\mathrm{LAI} > 2$ (38%) over the Bigfoot site (Northern Old Black Spruce, Manitoba, Canada) in the middle of boreal summer. Myneni *et al.* [13] estimated that classification errors in land cover maps can generate an LAI estimation error of up to 50%.

The third source of uncertainty is related to the different LAI algorithms used in LAI retrieval. Generally, two kinds of methods are applied to estimate LAI using remote sensing data; i.e., statistical methods [27]–[29], and inversion of physical models [13], [14]. Differences in vegetation structure, land cover, background reflectance, and local topography representation in the LAI algorithms will lead to substantial discrepancies in the final LAI retrievals [11], [30]–[32]. Previous inter-comparisons have shown that GLOBCARBON gives reliable and consistent seasonal and interannual variations [11], and agrees well with Landsat/ETM^{+} LAI maps at most test sites [4], [33]–[35]. Pisek and Chen [4] reported that the median relative absolute error of GLOBCARBON retrievals varied from 24% to 75% at the 1-km scale, compared with 34%–88% for MODIS standard LAI. However, GLOBCARBON tends to underestimate LAI over cropland and grassland, and can exhibit temporal instability during the growing season over evergreen forest sites [36], [11]. The first version of the GLOBCARBON LAI product has also been shown to perform poorly in mountainous areas; the second version includes improvements based on pixel-by-pixel consideration of local topography, clumping index, and background reflectance variations [32].

As the GLOBCARBON LAI algorithm has been validated and evaluated in several comprehensive studies in Canada, China, and other regions, we focus on its use with the new reflectance dataset from FY-3A/MERSI. We perform further inter-comparison, validation, and analysis of the uncertainties in MERSI GLOBCARBON LAI retrieval using both MODIS LSR-derived LAI using the same algorithm (MODIS GLOBCARBON LAI) and field LAI measurements. A case study was conducted over mainland China with the following objectives: (1) to compare the spatial and temporal performance of LAI retrievals from MERSI and MODIS LSR products using GLOBCARBON, (2) to validate and inter-compare MERSI GLOBCARBON LAI with field LAI measurements and other LAI products, and (3) to compare the two LSR data sets and the corresponding level 1 data (TOA reflectance) and further discuss the effect of the uncertainty in MERSI LSR data on LAI estimation.

II. Data

A. Data for LAI Retrieval

1) MERSI Land Surface Reflectance Data: FY-3A/MERSI LSR data for 2010 were downloaded from the National Satellite Meteorological center of China (NSMC) for FY-3A/MERSI LAI retrieval. It has 5 channels with 250 m spatial resolution and 15 channels with 1-km resolution. MERSI LSR is obtained from channels 1–4 of the MERSI 1B product after correction for gaseous absorption, Rayleigh and aerosol scattering, as well as interactions between these processes. Radiative transfer model simulations are used to establish look-up tables (LUTs). Parameters used in the atmospheric correction are interpolated from the pre-established LUTs [17] to achieve a pixel-by-pixel atmospheric correction. Ten-day composites were generated from daily MERSI LSR data for LAI retrieval.

2) MODIS Land Surface Reflectance Data: As the MODIS is one of the most frequently used sensors for LAI retrieval [37], [19], [11], we have chosen MODIS 8-day synthesis surface reflectance products (MOD09) for comparison with and evaluation of the FY-3A/MERSI LAI product. MOD09 corrects for the effects of atmospheric gases, aerosols, and thin cirrus clouds, and is an estimate of the land surface spectral reflectance [23]. MOD09A1 data with 500 m spatial resolution downloaded from NASA's Earth Observing System Data and Information System (EOSDIS) for 2010 were re-projected to geographic latitude/longitude and re-sampled to 1-km resolution for LAI retrieval.

3) Land Cover Data: A land cover map downloaded from the Global Land Cover 2000 database (GLC-2000) is used as an input for LAI retrieval. The GLC-2000 map uses 22 classes based on the Food and Agriculture Organization of the United Nations' hierarchical Land Cover Classification System [38]. This land cover product was adapted for use in the GLOBCARBON LAI algorithm. Some of the cover types with similar structural characteristics were combined, and snow and water body classes were ignored [14].

The spatial agreement of MERSI and MODIS GLOBCARBON LAI was investigated over mainland China and four test sites were selected with different land cover types to further compare the temporal variations of LAI (Fig. 1(a)). These sites are DBF (deciduous broadleaf forest area in the northeast of China, centered at 51.79°N, 121.06°E), DNF (deciduous needleleaf forest area in the northeast of China, centered at 51.78°N, 121.08°E), GLX (grassland in the Xilin Gol prairie of China, centered at 44.14°N, 116.29°E), and CLS (cropland in Yucheng, Shandong province of China, centered at 39.13°N, 115.67°E).

B. Data for Validation

Field LAI measurements were collected in a typical meadow grassland in the Hulunbeier prairie in China (centered at 49.41°N, 119.99°E) during June 21–26, 2010 [40]. Fifty-two 50×50 m sample plots, which have LAI values of 0.46 to 3.08, with a mean value of 1.74 and a standard deviation of 0.61, were set up (Fig. 1(b)). These sample plots are located in homogeneous locations with areas larger than 100×100 m so as to reduce the impact of topography and inhomogeneous land surface. In the center of each sample plot, two observation lines, parallel to the sun line and 25 m apart, were defined, and LAI data were collected using the LAI 2000 instrument along these lines (Fig. 1(c)). This sampling method resulted in 12 LAI measurements for each sample plot, which were then averaged to give the final LAI value for the specified sample plot.

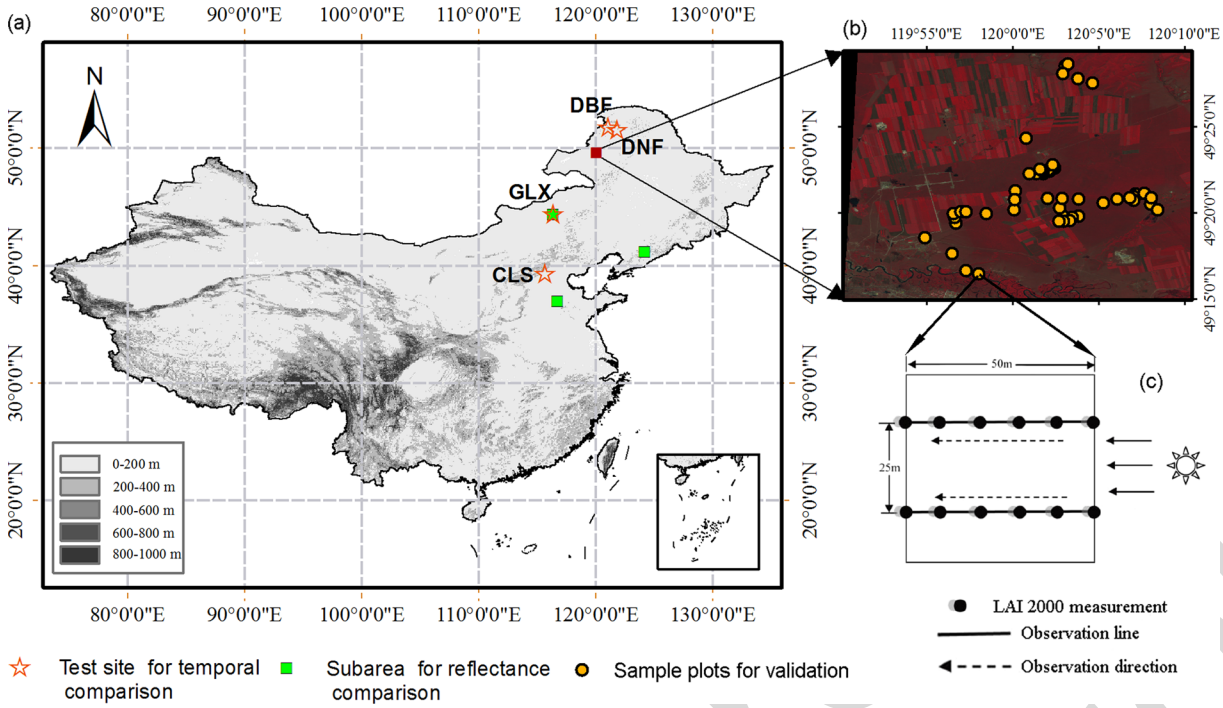

Fig. 1. (a) Map of the relief amplitude over the study area and locations of subarea and test sites for reflectance and temporal comparisons. (b) Locations of field LAI sample plots in a 30-m resolution false color composite map based on TM data. (c) Arrangement of LAI point measurements in a sample plot [40].

TABLE I
DATA SOURCES FOR FIELD VALIDATION AND INTER-COMPARISON OF DIFFERENT LAI PRODUCTS

Dataset name	*Date (Day of year, 2010)*	*Sensor used*	*Product used*	**LAI algorithm**
LAI_{MERSI}	169–176	FY-3A-MERSI	LSR	GLOBCARBON, an inversion model based on the 4-scale geometric optical model (Chen et al., 2002; Deng et al., 2006)
$LAI_{MOD09A1}$	169–176	Terra-MODIS	LSR (MOD09A1)	same as above
$LAI_{MOD15A2}$	169–176	Terra-MODIS	LSR (MOD15A21)	Main algorithm: an inversion model based on a three-dimensional canopy radiative transfer model (Myneni et al., 2002). Backup algorithm: biome-specific relations between NDVI and LAI.
LAI_{TM}	172	Landsat-5 TM	LSR	Site-specific empirical transfer function based on field LAI measurements over Hulunbeier prairie of China (Liu et al., 2011)

A satellite overpass scene (Landsat-5 TM) from 21 June 2010 was selected as the temporally closest cloud-free match to the field measurements (21–26 June 2010). The Landsat-5 TM image was downloaded from the United States Geological Survey (USGS) and converted to TOA radiance using the metadata provided in the TM data header. An atmospheric correction code (6S) [39] was used to convert TOA radiance to land surface reflectance. A vegetation index, Simple Ratio (SR; calculated from Landsat-5 TM data after atmospheric correction) was then correlated with field LAI measurements using an empirical linear function ($R^2 = 0.604$, $RMSE = 0.505$) [40].

To broaden the evaluation of FY-3A/MERSI LAI products, two other LAI products derived from MODIS 8-day synthesis data (MOD09A1 & MOD15A2) were also evaluated. Table I lists the data sources and algorithms for FY-3A/MERSI LAI validation and inter-comparison. All LAI products are re-sampled to 3-km resolution so as to further reduce the influence of image geolocation errors. There are 282 points in total, randomly selected around the LAI field measurement site, and scatter plots were generated to demonstrate the correlation between each pair of LAI products.

C. Data for Uncertainty Analysis

1) Reflectance Data: Four types of remote sensing data were used for the inter-comparison of spectral reflectance between sensors: (a) the MODIS level 1B TOA reflectance product, (b) the corresponding daily LSR products (MYD09GA) downloaded from EOSDIS, (c) the contemporaneous MERSI level

TABLE II
DATA USED FOR REFLECTANCE COMPARISON

Sensor type	Product type	Acquisition dates	Longitude	Latitude	Land cover type
FY-3A/MERSI	Daily TOA reflectance	5-Jun-10	123.84–124.33 °E	40.38–40.88 °N	Broadleaf forest
FY-3A/MERSI	Daily LSR reflectance	5-Jun-10	123.84–124.33 °E	40.38–40.88 °N	
Terra/MODIS	TOA reflectance	5-Jun-10	123.84–124.33 °E	40.38–40.88 °N	
FY-3A/MERSI	Daily TOA reflectance	26-Jun-10	116.08–116.58 °E	44.39–44.44 °N	Grassland
FY-3A/MERSI	Daily LSR reflectance	26-Jun-10	116.08–116.58 °E	44.39–44.44 °N	
Terra/MODIS	TOA reflectance	26-Jun-10	116.08–116.58 °E	44.39–44.44 °N	
Terra/MODIS	LSR reflectance (MYD09GA)	26-Jun-10	116.08–116.58 °E	44.39–44.44 °N	
FY-3A/MERSI	Daily TOA reflectance	25-May-10	116.38–116.91 °E	37.23–37.79 °N	Cropland
FY-3A/MERSI	Daily LSR reflectance	25-May-10	116.38–116.91 °E	37.23–37.79 °N	
Terra/MODIS	TOA reflectance	25-May-10	116.38–116.91 °E	37.23–37.79 °N	
Terra/MODIS	LSR reflectance (MYD09GA)	25-May-10	116.38–116.91 °E	37.23–37.79 °N	

1B TOA reflectance, and (d) the corresponding daily LSR products with 1-km resolution distributed by NSMC. MERSI and MODIS TOA and LSR products were all co-registered and aggregated to 1-km resolution.

MERSI and MODIS 1B and LSR products were chosen over three typical areas with adjacent overpass times, small zenith view angles, and cloud-free conditions. The acquisition dates, position, land cover types, and observation geometry for the selected MERSI and MODIS TOA reflectance and LSR images are given in Table II.

D. Topographic Data

A relief amplitude map (Fig. 1(a)) of the study area is used to describe quantitatively the influence of topographic characteristics on LAI retrieval. The map was generated using a digital elevation model (DEM; SRTM 4.1, Shuttle Radar Topography Mission) and the neighborhood statistics function of ArcGIS [41]. Relief amplitude is defined as the vertical difference in elevation between the highest and lowest points for a particular area (3×3 pixels, with 1-km resolution), and is used to quantify the localized changes in terrain across the landscape. As shown in Fig. 1(a), the relief amplitude in most of the study area is less than 400 m. However, in southwest China, the relief amplitude increases up to 1000 m, indicating large slopes in this area.

III. METHOD

A. GLOBCARBON LAI Algorithm

The European Space Agency funded GLOBCARBON, an initiative to produce multi-year global Level 3 land products that include LAI [42], for the purpose of global carbon cycle modeling [3]. Products derived from data from the VEGETATION instrument, the Along Track Scanning Radiometers (AATSR and ATSR-2), and the Medium Resolution Imaging Spectrometer (MERIS) are available for the period 1998–2007. GLOBCARBON uses a geometric optical model (Four-Scale model) [30] with a multiple scattering scheme [43] and LAI algorithms previously derived for Canada-wide applications [10] to establish angle-specific relationships between Simple Ratio (SR) and LAI, and between Reduced SR (RSR) and LAI for various land cover types [14].

SR and RSR are the starting points for LAI retrieval and can be expressed as

$$\mathrm{SR} = \frac{\rho_{\mathrm{NIR}}}{\rho_{\mathrm{Red}}} \tag{1}$$

where ρ_{NIR} and ρ_{Red} are the reflectances in the near infrared and red bands, respectively.

RSR is defined as

$$\mathrm{RSR} = \frac{\rho_{\mathrm{NIR}}}{\rho_{\mathrm{Red}}} \left(1 - \frac{\rho_{SWIR} - \rho_{SWIR_{\min}}}{\rho_{SWIR_{\max}} - \rho_{SWIR_{\min}}}\right) \tag{2}$$

where ρ_{SWIR} is the reflectance in the SWIR band and $\rho_{SWIR_{\max}}$ and $\rho_{SWIR_{\min}}$ are the maximum and minimum SWIR reflectances for specific land covers, respectively [44], [14].

Bidirectional reflectance distribution function (BRDF), land cover, foliage clumping, and soil background effects are all explicitly considered in GLOBCARBON algorithm through Four-Scale model simulations. Relationships between SR and LAI over large ranges of viewing and illumination angles and land cover types can be expressed as

$$\mathrm{LAI} = f_{L\_SR}(\mathrm{SR} \cdot f_{BRDF}(\theta_v, \theta_s, \varphi)) \tag{3}$$

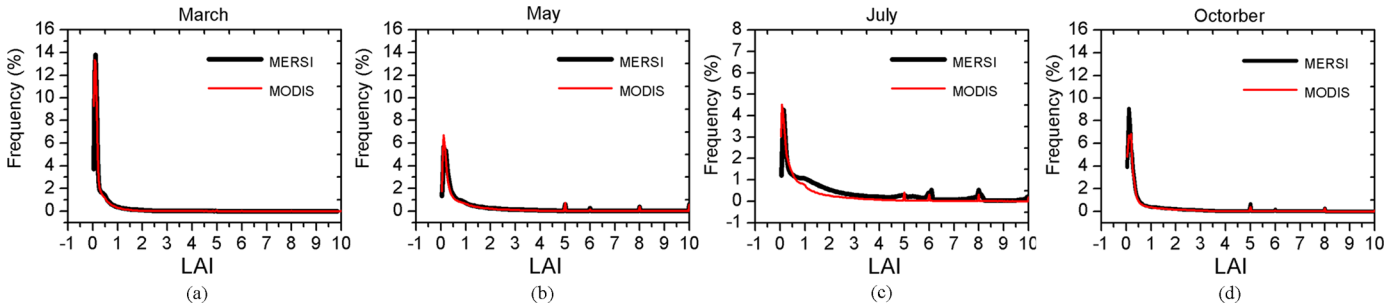

Fig. 2. Comparison of LAI value distribution over China for (a) March, (b) May, (c) July, and (d) October of 2010.

where θ_s is the solar zenith angle (SZA), θ_v is the view zenith angle (VZA), φ is the relative azimuth angle, $f_{BRDF}()$ is the BRDF modification function for SR, and $f_{L\_SR}()$ is a function describing the relationship between BRDF-modified SR and LAI.

Similarly, LAI–RSR relationships have been established as follows [14]

$$\mathrm{LAI} = f_{L\_RSR}\left(\mathrm{SR}\cdot f_{BRDF}(\theta_v,\theta_s,\varphi) \cdot\left(1-\frac{\rho_{SWIR}\cdot f_{SWIR\_BRDF}(\theta_v,\theta_s,\varphi)-\rho_{\mathrm{SWIRmin}}}{\rho_{\mathrm{SWIRmax}}-\rho_{\mathrm{SWIRmin}}}\right)\right) \tag{4}$$

where $f_{L\_RSR}()$ is a function describing the relationship between BRDF-modified RSR and LAI, and $f_{SWIR\_BRDF}()$ is a BRDF modification function for SWIR reflectance. The use of the SWIR band in RSR gives LAI-RSR relationships that minimize the variable background effect on LAI retrieval over forest [14].

To further minimize residual atmospheric effects, GLOBCARBON uses a procedure known as Locally Adjusted Cubic-spline Capping (LACC) [3] to reconstruct the seasonal trajectory of LAI. In LACC, a variable local smoothing parameter is automatically determined according to the local curvature of the original seasonal variation pattern. The final optimal solution is obtained from an iteration procedure by progressively replacing anomalously low values with fitted values [3].

B. Spatial Agreement Analysis Method

The spatial agreement of MERSI GLOBCARBON LAI and MODIS GLOBCARBON LAI is evaluated using an agreement index [45] defined as

$$A_{index} = 1 - \frac{\sum_{k=1}^{n}(P_k - O_k)^2}{\sum_{k=1}^{n}\left[(|P'_k| + |O'_k|)^2\right]} \tag{5}$$

where $P'_k = P_k - \overline{O}$ and $O'_k = O_k - \overline{O}$, O are observations, P are model predictions, $\overline{O}$ represents the observed mean, and n is the number of matching pairs over the study period. The agreement index (A_{index}) ranges from 0 to 1; i.e., from no agreement to perfect agreement between observation and prediction. In the present study, O represents MERSI GLOBCARBON LAI and P represents MODIS GLOBCARBON LAI at the same location and same time, and $n = 5$ matching pairs in 2010 (8-day synthesis LAI retrievals: 9–10 January, 22–30 March, 17–24 May, 20–27 July, and 24–31 October).

IV. Results and Discussion

A. Comparison of MERSI and MODIS GLOBCARBON LAI

1) Spatial Frequency: Fig. 2(a)–(d) displays the LAI histograms for MERSI GLOBCARBON LAI and MODIS GLOBCARBON LAI in four specific months (March, May, July, and October 2010) that cover the main vegetation growing period. Frequency is given as a percentage of the total number of pixels over mainland China.

Both MERSI GLOBCARBON LAI and MODIS GLOBCARBON LAI show continuous and smooth frequency distributions in March (as shown in Fig. 2(a)). MODIS has a higher frequency of retrievals at low LAI values (LAI less than 0.04). During May and October, these two LAI products also show continuous smooth frequency patterns except for several small peaks at LAI values 5, 6, and 8, which are artifacts associated with the maximum LAI limits in the GLOBCARBON LAI algorithm for different land cover types. The largest LAI differences between these two products occur at the peak of the growing season during July (Fig. 2(c)), when MERSI shows a much higher frequency of retrievals with LAI greater than 0.75 than does MODIS. For both LAI products, the frequency of low LAI values is very high at the start and end of the growing season, and decreases during the peak growing season, which is consistent with other LAI products and is in agreement with vegetation growth over northern latitudes [11].

2) Spatial Agreement: The spatial performance of the MERSI and MODIS retrievals using the GLOBCARBON algorithm over mainland China from January to October 2010 is shown in Fig. 3. The agreement index is larger than 0.8 (0.6) for 38.85% (63.17%) of the land area in mainland China, suggesting that in most locations, LAI retrievals from MERSI and MODIS agree well. However, some low values of agreement index are found in southeast China due to frequent cloud cover that influences MERSI and MODIS reflectance differently.

3) Temporal Variations: The temporal variations of MERSI GLOBCARBON LAI and MODIS GLOBCARBON LAI over four test sites (Fig. 1) with different land cover types were compared for a full year in 2010. As shown in Fig. 4(a), over DBF, MERSI GLOBCARBON LAI and MODIS GLOBCARBON LAI have similar trends, especially during the growing season,

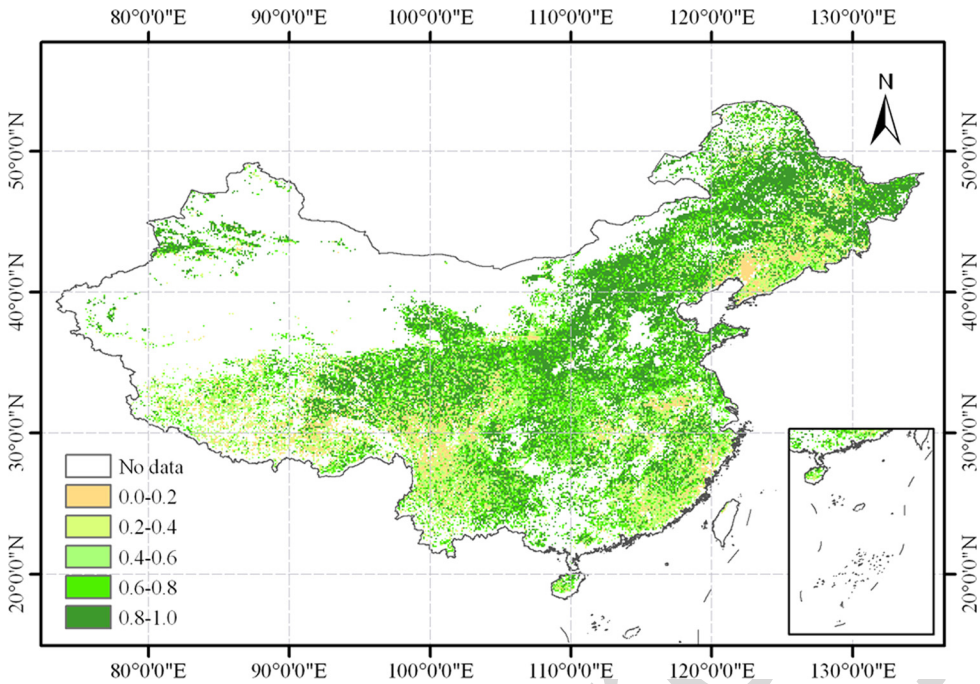

Fig. 3. Agreement index between MERSI GLOBCARBON LAI and MODIS GLOBCARBON LAI using 5 matching pairs of 8-day synthesis LAI retrievals in 2010 (9–10 January, 22–30 March, 17–24 May, 20–27 July and 24–31 October).

but their magnitudes differ during the peak growing season. At the end of the growing season, MERSI GLOBCARBON LAI decreases earlier than MODIS GLOBCARBON LAI. It is also obvious that there are several anomalously low LAI values in MODIS and MERSI LAI trajectories due to the remaining effects of cloud and aerosol on multi-day composite reflectance data. We can also see the improvement in MERSI GLOBCARBON LAI after applying LACC smoothing. Erratic LAI values in MERSI GLOBCARBON LAI trajectories were corrected, giving a smoother seasonal variation of LAI that better resembles the expected variation in vegetation growth. At the peak of the growing season, there are distinct differences between MERSI GLOBCARBON LAI and MODIS GLOBCARBON LAI. An earlier study has shown that the maximum LAI for broadleaf forest is 4–6 in northeast China [46]. For broadleaf forests, MERSI GLOBCARBON LAI is larger than MODIS GLOBCARBON LAI.

Over DNF (Fig. 4(b)), MODIS and MERSI GLOBCARBON LAI retrievals are similar but both seem to overestimate LAI. Considering that the same LAI algorithm was used for MERSI and MODIS, the biases of these LAI products may be caused by uncertainties in the atmospheric correction process and the difference in spectral response functions between the two sensors. For dense canopies in particular, near infrared reflectance saturates at moderate LAI values (2–4), and a very small bias in the red band reflectance due to error in atmospheric correction will lead to a significant bias in vegetation index, which tends to destabilize the LAI retrieval [11].

Over GLX (Fig. 4(c)), MERSI GLOBCARBON LAI and MODIS GLOBCARBON LAI follow the beginning and the end of the season reasonably well, but from day of year 120, MODIS GLOBCARBON LAI begins to diverge from MERSI GLOBCARBON LAI. During the peak growing season, MODIS GLOBCARBON LAI is lower than MERSI GLOBCARBON LAI. The typical LAI value for GLX in the same area is 1–3 from ecosystem model simulation and field LAI observations [36]. Considering the mixed pixel effect from field scale to regional scale, the actual LAI retrieved from moderate resolution remote sensing data is expected to be lower.

Over CLS (Fig. 4(d)), both MERSI GLOBCARBON LAI and MODIS GLOBCARBON LAI display a two-peak pattern, which is a fair representation of the succession between winter wheat and summer corn. During the peak of winter wheat growth, MERSI GLOBCARBON LAI is a little higher than MODIS GLOBCARBON LAI, whereas during the peak of summer corn growth, MODIS GLOBCARBON LAI attains an anomalously high value, which is possibly related to the erratic land surface reflectance due to the remaining atmospheric effects. The start and end of the growing season for MODIS GLOBCARBON LAI do not coincide with those for MERSI GLOBCARBON LAI. This is possibly due to different composite periods for the two LAI products. MERSI GLOBCARBON LAI is computed from 10-day composites of MERSI LSR images using the maximum normalized difference vegetation index (NDVI) criterion, whereas MODIS GLOBCARBON LAI was calculated from 8-day cloud-free composites of MODIS LSR images.

B. Validation

Fig. 5(a)–(c) compares LAI derived from moderate resolution sensors including MERSI and MODIS with measured LAI aggregated to 3-km resolution using TM data ($\mathrm{LAI_{TM}}$). Although the different LAI data generally vary in a similar fashion, the scatter of data points is considerable (SD ranges from 0.36 to 0.51). In Fig. 5(a) and (b), even though the same LAI algorithm was used for $\mathrm{LAI_{MERSI}}$ and $\mathrm{LAI_{MOD09A1}}$, uncertainties in the

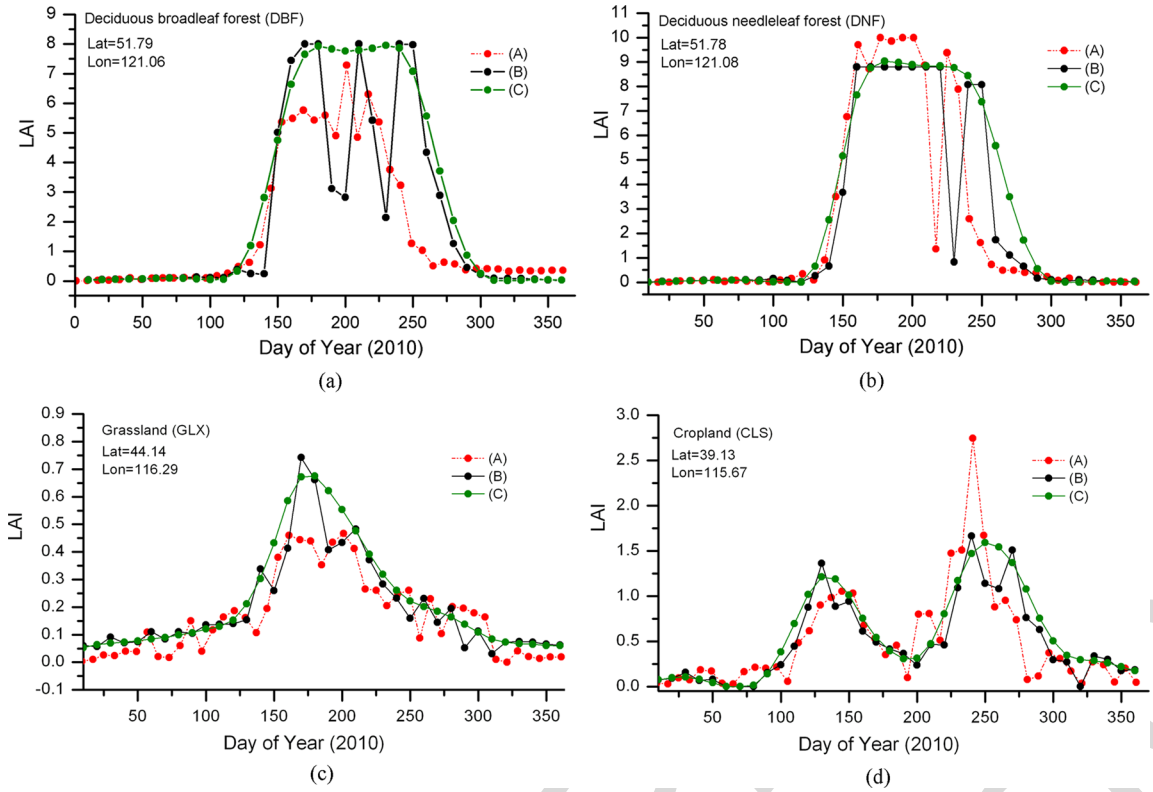

Fig. 4. Seasonal variations in MERSI GLOBCARBON LAI and MODIS GLOBCARBON LAI for (a) deciduous broadleaf forest, (b) deciduous needleleaf forest, (c) grassland, and (d) cropland. (A) Red dots represent MODIS GLOBCARBON LAI without LACC smoothing, (B) black dots represent MERSI GLOBCARBON LAI without LACC smoothing, and (C) green dots represent MERSI GLOBCARBON LAI with LACC smoothing.

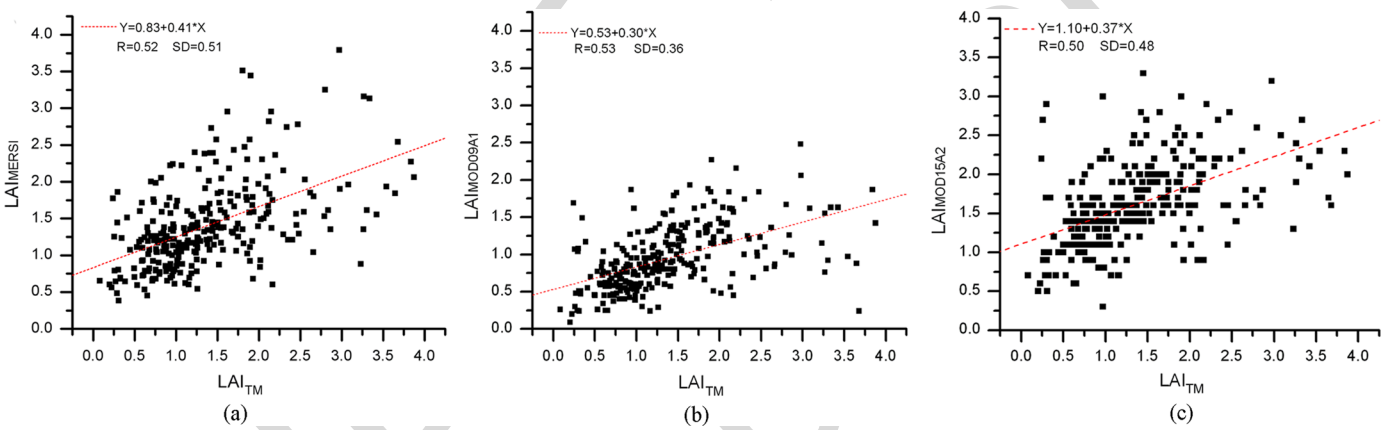

Fig. 5. Inter-comparison and validation of MERSI LAI and other LAI products: (a) MERSI GLOBCARBON LAI vs. TM LAI, (b) MODIS GLOBCARBON LAI vs. TM LAI, and (c) MODIS standard LAI product vs. TM LAI.

atmospheric correction process for MERSI and MODIS images possibly contribute to the large differences between the final LAI retrievals. The slight difference between $\mathrm{LAI}_{\mathrm{MOD09A1}}$ and $\mathrm{LAI}_{\mathrm{MOD15A21}}$ performance compared with $\mathrm{LAI}_{\mathrm{TM}}$, however, can be attributed to the different LAI algorithms used in LAI retrieval. The correlation coefficient R varies slightly from 0.50 to 0.53 in Fig. 5(a) to (c), suggesting that the three LAI products (i.e., $\mathrm{LAI}_{\mathrm{MERSI}}$, $\mathrm{LAI}_{\mathrm{MOD09A1}}$ and $\mathrm{LAI}_{\mathrm{MOD15A21}}$), which use two different LAI algorithms and data from two different sensors, have comparable accuracy relative to the high resolution aggregated LAI ($\mathrm{LAI}_{\mathrm{TM}}$) over grassland.

C. *Uncertainty Analysis*

1) Influence of Input Reflectance: Vegetation indices (SR or RSR) derived from red, near infrared, and shortwave infrared reflectance are the starting point for LAI calculation with the GLOBCARBON LAI algorithm. SR is more sensitive to atmospheric conditions than is RSR. The influence of the atmospheric correction procedure on the final accuracy of LAI was investigated further using scatter plots between MODIS and MERSI TOA-reflectance-derived SR and LSR-derived SR for three typical areas of China with different land cover types.

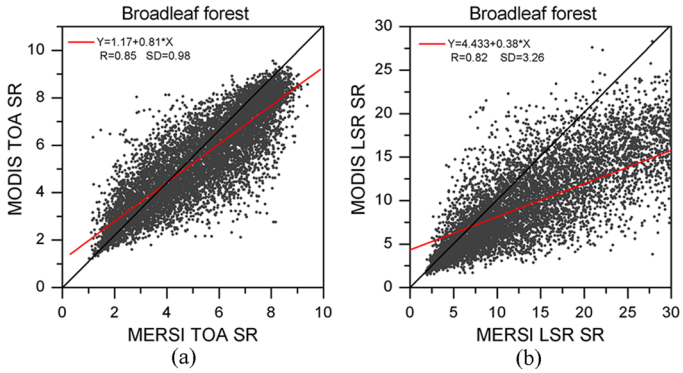

Fig. 6. Scatter plot between MERSI and MODIS data over broadleaf forest area for (a) TOA reflectance and (b) LSR.

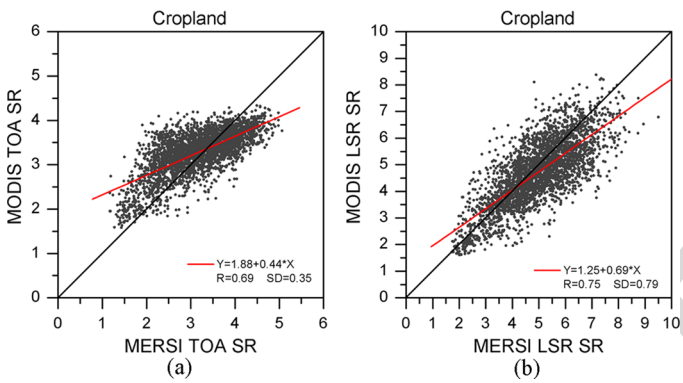

Fig. 7. Scatter plot between MERSI and MODIS data over cropland for (a) TOA reflectance and (b) LSR.

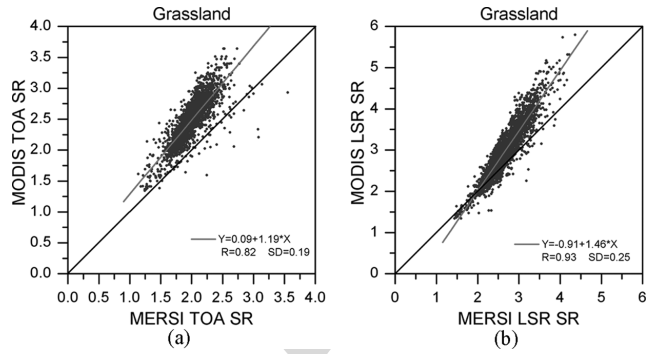

Fig. 8. Scatter plot between MERSI and MODIS data over grassland for (a) TOA reflectance and (b) LSR.

It is encouraging that MODIS TOA SR and MERSI TOA SR are well correlated for all three land cover types, with linear correlation coefficients higher than 0.6 (as shown in Figs. 6–8). The lowest correlation coefficient (R) of up to 0.69 is found over cropland and the maximum R of up to 0.82 is found over grassland, showing the comparable capability and quality of MERSI and MODIS for vegetation monitoring. The regression slope mainly shows differences between MERSI and MODIS due to the spectral response and point spread functions. After atmospheric correction, the relationship between MODIS LSR SR and MERSI LSR SR is slightly better than that between MODIS TOA SR and MERSI TOA SR for grassland and cropland, although by different degrees (R increases from 0.82 to 0.93 over grassland and from 0.69 to 0.75 over cropland), suggesting that using the ratio of the red and NIR spectral bands can effectively reduce the influence of atmospheric contamination.

However, atmospheric correction is still one of the main causes of scatter between data from the two sensors. As shown in Figs. 6–8, for different land cover types, the SD values are all higher after atmospheric correction. The highest SD value is observed over forest (Fig. 6(b)). According to the Four-scale simulations, the shadow effect of forest will reduce the red band reflectance, while strengthening multiple scattering of the NIR band radiation, shifting the saturation of SR signals to higher LAI values [10]. Therefore, while the forest shadow effect makes the final MERSI LAI higher than MODIS LAI during the peak growing season for broadleaf forests (as shown in Fig. 6(a)–(c)), it also tends to introduce large uncertainty in the red band during atmospheric correction and greatly influences the SR value, increasing the scatter among the data points (Fig. 6(b)).

Apart from atmospheric contamination and land cover, the mixed pixel effect, acquisition time difference, and geo-location are all potential factors causing large scatter around the regression line. As shown in Fig. 6(a), over forest, the data scatter is greatest in the center of the plot, indicating mixed pixels. Over grassland, MODIS SR is generally higher than MERSI. This disagrees with the result of Fig. 4(c) where MERSI LAI is higher than MODIS LAI during the growing season. In Fig. 4, 10-day MERSI LSR composite images and 8-day MODIS LSR composite images are used for comparing the temporal variation, whereas in Fig. 6 only one scene is used. This result reinforces the view that differences in image acquisition date are another major reason for discrepancies between MODIS SR and MERSI SR, as shown in previous studies (e.g., [4]).

2) Influence of Land Cover Type and Topography: The frequency of pixels with agreement index greater than 0.5 for different land cover types and relief amplitude index values are shown in Figs. 9 and 10, respectively. For most land cover types, more than 72% of pixels have an agreement index greater than 0.5, suggesting that MERSI GLOBCARBON LAI and MODIS GLOBCARBON LAI agree well in space and time. Compared with other land cover types, grassland has the highest frequency of high values (> 0.5). This result is consistent with the fact that MERSI SR and MODIS SR have the highest linear correlation coefficient (R) over grassland, as shown in Section IV.C.1. In the case of broadleaf and mixed forest, the greatest disagreement arises from the significant overestimate of SR by MERSI LSR (as shown in Fig. 6(b)), which results in large numbers of upper bound LAI values in the MERSI GLOBCARBON LAI.

The spatial variation of is better correlated with the relief amplitude index (Fig. 10) than with land cover type. As the relief amplitude index increases, the frequency of > 0.5 decreases. Uncertainty in the estimation of surface reflectance is a major contributor to this variation. MODIS and MERSI LSR products all use a Lambertian surface approximation for atmospheric correction instead of a BRDF correction process [23], [17], which will reduce the accuracy of the LSR product, especially in hilly

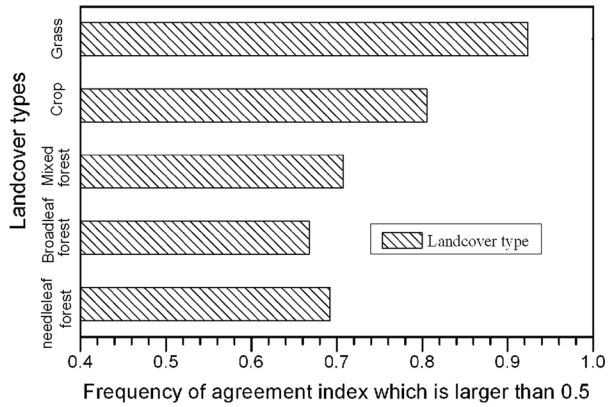

Fig. 9. Frequency of agreement index greater than 0.5 for different land cover types.

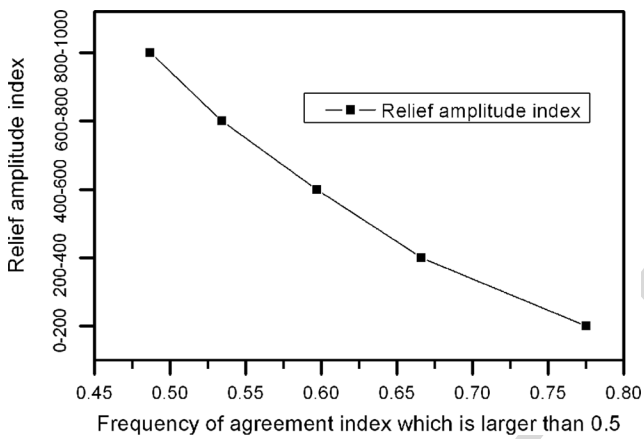

Fig. 10. Frequency of agreement index greater than 0.5 for different relief amplitude indexes.

areas [11]. The complex terrain effect may introduce uncertainties into the atmospheric correction process, and therefore increases the discrepancy between the two LAI products.

V. Summary and Conclusion

In this study, the spatial and temporal performance of the FY-3A/MERSI LSR product for LAI retrieval using the GLOBCARBON LAI algorithm are inter-compared and validated with MODIS LSR derived LAI and field LAI measurements over mainland China. The influence of input reflectance, land cover type, and topography on the final accuracy of LAI are further explored and discussed. The following conclusions are drawn.

a) MERSI GLOBCARBON LAI and MODIS GLOBCARBON LAI show a continuous and smooth LAI distribution at the start and end of the growing season. These two LAI products agree well, with an agreement index greater than 0.5, over 72.08% of mainland China. The largest LAI difference occurs during July, MERSI shows a much higher frequency of retrievals than does MODIS. The overestimate of MERIS GLOBCARBON LAI in the peak growing season is mainly due to the overestimate of SR derived from MERSI-LSR in dense canopies, causing a mismatch between the reflectance modeled by the LAI algorithm and the MERSI derived land surface reflectance.

b) Our study demonstrates that LAI values derived from MERSI LSR and MODIS LSR have comparable accuracy relative to an independent LAI map derived using a Landsat TM image (LAITM) in combination with ground LAI data. Of all the LAI values derived from MERSI and MODIS, MODIS GLOBCARBON LAI has the best correlation with LAITM ($R = 0.53$). This result indicates that the GLOBCARBON LAI algorithm performs slightly better than the standard MODIS LAI algorithm, which is based mainly on a radiative transfer model.

c) There are good relationships between MODIS TOA SR and MERSI TOA SR for all three land cover types, with linear correlation coefficients greater than 0.6. By taking the ratio between the red and NIR spectral bands, SR can effectively reduce the influence of atmospheric contamination. However, atmospheric correction is still a cause of scatter among data from the two sensors.

d) Different land cover types and different terrain relief index values have contrasting influences on the atmospheric correction, and these influences reduce the agreement between MODIS and MERSI GLOBCARBON LAI.

This study focused solely on mainland China, and limited field measurement data were used for LAI product evaluation. Global use of MERSI GLOBCARBON LAI products will require additional validation in other areas. Furthermore, in the Results and Discussion sections, we made a special effort to discuss the uncertainty in the LAI–SR relationship of the GLOBCARBON algorithm. It is also important to show how MERSI and MODIS SWIR reflectance relate to each other since the GLOBCARBON algorithm also relies on SWIR reflectance. We will investigate these considerations in future work. This study shows the great potential of FY-3A/MERSI LAI for global vegetation monitoring and for further effective use in ecosystem modeling.

Acknowledgment

The authors are most grateful to Prof. W. M. Ju and Dr. Y. Liu of Nanjing University, China, for help with field LAI measurement collection and LAI validation, and to two anonymous reviewers for constructive comments that greatly improved the manuscript.

References

[1] G. B. Bonan, "Land-atmospheric interactions for climate system models: Coupling biophysical, biogeochemical and ecosystem dynamical processes," *Remote Sens. Environ.*, vol. 51, no. 1, pp. 57–73, Jan. 1995.

[2] P. J. Sellers, F. G. Hall, R. D. Kelley, A. Black, D. Baldocchi, J. Berry, M. Ryan, K. J. Ranson, P. M. Crill, D. P. Lettenmaier, H. Margolis, J. Cihlar, J. Newcomer, D. Fitzjarrald, P. G. Jarvis, S. T. Gower, D. Halliwell, D. Williams, B. Goodison, D. E. Wickland, and F. E. Guertin, "BOREAS in 1997: Experiment overview, scientific results, and future directions," *J. Geophys. Res.*, vol. 102, no. D24, pp. 28731–28769, Dec. 1997.

[3] J. M. Chen, F. Deng, and M. Chen, "Locally adjusted cubic-spline capping for reconstructing seasonal trajectories of a satellite-derived surface parameter," *IEEE Trans. Geosci. Remote Sens.*, vol. 44, no. 8, pp. 2230–2238, Aug. 2006.

[4] J. Pisek and J. M. Chen, "Comparison and validation of MODIS and VEGETATION global LAI products over four BigFoot sites in North America," *Remote Sens. Environ.*, vol. 109, no. 1, pp. 81–94, Aug. 2007.

[5] N. C. Coops, R. H. Waring, and J. J. Landsberg, "Estimation of potential forest productivity across the Oregon transect using satellite data and monthly weather records," *Int. J. Remote Sens.*, vol. 22, no. 18, pp. 3797–3812, 2001.

[6] J. M. Chen and T. A. Black, "Defining leaf-area index for nonflat leaves," *Plant Cell Environ.*, vol. 15, no. 4, pp. 421–429, May 1992.

[7] M. Weiss, F. Baret, G. Smith, I. Jonckheere, and P. Coppin, "Review of methods for in situ leaf area index (LAI) determination, Part II. Estimation of LAI, errors and sampling," *Agr. Forest Meteorol.*, vol. 121, no. 1–4, pp. 37–53, Jan. 2004.

[8] G. B. Bonan, "Forests and climate change: Forcings, feedbacks, and the climate benefits of forests," *Science*, vol. 320, no. 5882, pp. 1444–1449, Jun. 2008.

[9] Implementation Plan for the Global Observing System for Climate in Support of the UNFCCC, WMO, 2010, GCOS Report No. 138, GOOS Report No. 184 (WMO- TD/No. 1523).

[10] J. M. Chen, G. Pavlic, L. Brown, J. Cihlar, S. G. Leblanc, H. P. White, R. J. Hall, D. R. Peddle, D. J. King, J. A. Trofymow, E. Swift, J. Van der Sanden, and P. K. E. Pellikka, "Derivation and validation of Canada-wide coarse-resolution leaf area index maps using high-resolution satellite imagery and ground measurements," *Remote Sens. Environ.*, vol. 80, no. 1, pp. 165–184, Apr. 2002.

[11] S. Garrigues, R. Lacaze, F. Baret, J. T. Morisette, M. Weiss, J. E. Nickeson, R. Fernandes, S. Plummer, N. V. Shabanov, R. B. Myneni, Y. Knyazikhin, and W. Yang, "Validation and intercomparison of global leaf area index products derived from remote sensing data," *J. Geophys. Res., Biogeosci.*, vol. 113, no. G2, pp. 1–20, Jun. 2008.

[12] P. J. Sellers, S. O. Los, C. J. Tucker, C. O. Justice, D. A. Dazlich, G. J. Collatz, and D. A. Randall, "A revised land surface parameterization (SiB2) for atmospheric GCMS. Part II: The generation of global fields of terrestrial biophysical parameters from satellite data," *J. Clim.*, vol. 9, no. 4, pp. 706–737, Apr. 1996.

[13] R. B. Myneni, Y. Knyazikhin, J. L. Privette, J. Glassy, Y. Tian, Y. Wang, X. Song, Y. Zhang, G. R. Smith, A. Lotsch, M. Friedl, J. T. Moriestte, P. Votava, R. R. Nemani, and S. W. Running, "Global products of vegetation leaf area and fraction absorbed PAR from year one of MODIS data," *Remote Sens. Environ.*, vol. 83, no. 1–2, pp. 214–231, Feb. 2002.

[14] F. Deng, J. M. Chen, S. Plummer, and J. Pisek, "Algorithm for global leaf area index retrieval using satellite imagery," *IEEE Trans. Geosci. Remote Sens.*, vol. 44, no. 8, pp. 2219–2229, Aug. 2006.

[15] F. Baret, O. Hagolle, B. Geiger, P. Bicheron, B. Miras, M. Huc, B. Berthelot, F. Nino, M. Weiss, O. Samain, J. L. Roujean, and M. Leroy, "LAI, fAPAR and fCover CYCLOPES global products derived from VEGETATION, Part 1: Principles of the algorithm," *Remote Sens. Environ.*, vol. 110, no. 3, pp. 275–286, Oct. 2007.

[16] J. Yang, C. H. Dong, N. M. Lu, Z. D. Yang, J. M. Shi, P. Zhang, Y. J. Liu, and B. Cai, "FY-3A: The new generation polar-orbiting meteorological satellite of China," *Acta Meteorologica Sinica*, vol. 67, no. 4, pp. 501–509, Dec. 2009.

[17] J. Yang *et al.*, "MERSI land surface reflectance with 250 m resolution," in *Operational Products and Application of New Generation of FY Polar-Obit Meteorological Satellite*, 1st ed. Beijing, China: Science Press, 2011, pp. 250–252.

[18] C. Dong, J. Yang, W. Zhang, Z. Yang, N. Lu, J. Shi, P. Zhang, Y. Liu, and B. Cai, "An overview of a new Chinese weather satellite FY-3A," *Bull. Amer. Meteorol. Soc.*, vol. 90, no. 10, pp. 1531–1544, Oct. 2009.

[19] B. Tan, J. Hu, D. Huang, W. Yang, P. Zhang, N. V. Shabanov, Y. Knyazikhin, R. R. Nemani, and R. B. Myneni, "Assessment of the broadleaf crops leaf area index product from the Terra MODIS instrument," *Agr. Forest Meteorol.*, vol. 135, no. 1–4, pp. 124–134, Dec. 2005.

[20] Y. Yi, D. Yang, J. Huang, and D. Chen, "Evaluation of MODIS surface reflectance products for wheat leaf area index (LAI) retrieval," *Int. J. Remote Sens.*, vol. 63, no. 6, pp. 661–677, Nov. 2008.

[21] F. M. Bréon and E. Vermote, "Correction of MODIS surface reflectance time series for BRDF effects," *Remote Sens. Environ.*, vol. 125, pp. 1–9, Oct. 2012.

[22] E. Vermote, C. O. Justice, and F. M. Breon, "Towards a generalized approach for correction of the BRDF effect in MODIS directional reflectances," *IEEE Trans. Geosci. Remote Sens.*, vol. 47, no. 3, pp. 898–908, Mar. 2009.

[23] E. F. Vermote and A. Vermeulen, Atmospheric Correction Algorithm: Spectral Reflectances (MOD09), NASA, contract NAS5-96062, 1999 [Online]. Available: http://modis.gsfc.nasa.gov/data/atbd/atbd_mod08.pdf

[24] P. Maisongrande, B. Duchemin, and G. Dedieu, "VEGETATION/SPOT: An operational mission for the Earth monitoring; presentation of new standard products," *Int. J. Remote Sens.*, vol. 25, no. 1, pp. 9–14, Jan. 2004.

[25] J. M. Chen, "Spatial scaling of a remotely sensed surface parameter by contexture," *Remote Sens. Environ.*, vol. 69, no. 1, pp. 30–42, Jul. 1999.

[26] S. Garrigues, D. Allard, and F. Baret, "Influence of the spatial heterogeneity on the nonlinear estimation of Leaf Area Index from moderate resolution remote sensing data," *Remote Sens. Environ.*, vol. 105, no. 4, pp. 286–298, Dec. 2006.

[27] J. W. Rouse, R. H. Haas, J. A. Schell, and D. W. Deering, "Monitoring vegetation systems in the great plains with ERTS," in *Proc. 3rd ERTS Symp.*, 1973, vol. 1, pp. 309–317.

[28] J. M. Chen, "Evaluation of vegetation indices and a modified simple ratio for boreal application," *Can. J. Remote Sens.*, vol. 22, no. 3, pp. 229–242, Jan. 1996.

[29] F. M. Wang, J. F. Huang, Y. L. Tang, and X. Z. Wang, "New vegetation index and its application in estimating leaf area index of rice," *Chin. J. Rice Sci.*, vol. 21, no. 2, pp. 159–166, Sep. 2007.

[30] J. M. Chen and S. G. Leblanc, "A 4-scale bi-directional reflection model based on canopy architecture," *IEEE Trans. Geosci. Remote Sens.*, vol. 35, no. 5, pp. 1316–1337, Sep. 1997.

[31] K. Richter, C. Atzberger, F. Vuolo, and G. D'Urso, "Evaluation of Sentinel-2 spectral sampling for radiative transfer model based LAI estimation of wheat, sugar beet, and maize," *IEEE J. Sel. Topics Appl. Earth Observ. Remote Sens. (JSTARS)*, vol. 4, no. 2, pp. 458–464, Jun. 2011.

[32] A. Gonsamo and J. M. Chen, "Improved LAI algorithm implementation to MODIS data by incorporating background, topography, and foliage clumping information," *IEEE Trans. Geosci. Remote Sens.*, 2013, DOI: 10.1109/TGRS.2013.2247405.

[33] R. Liu, J. M. Chen, J. Liu, F. Deng, and R. Sun, "Application of a new leaf area index algorithm to China's landmass using MODIS data for carbon cycle research," *J. Environ. Manage.*, vol. 85, no. 3, pp. 649–658, Nov. 2007.

[34] X. F. Li, W. M. Ju, Y. L. Zhou, and S. Chen, "Retrieving leaf area index of forests in red soil hilly region using remote sensing data," in *Proc. SPIE 7471*, Oct. 2009.

[35] Y. B. Liu, W. M. Ju, J. M. Chen, G. L. Zhu, B. L. Xing, J. F. Zhu, and M. Z. He, "Spatial and temporal variations of forest LAI in China during 2000–2010," *Chin. Sci. Bull.*, vol. 57, no. 22, pp. 2846–2856, Aug. 2012.

[36] F. Camacho, J. Cemicharo, R. Lacaze, F. Baret, and M. Weiss, "GEOV1: LAI, FAPAR essential climate variables and FCOVER global time series capitalizing over existing products. Part 2: Validation and intercomparison with reference products," *Remote Sens. Environ.*, vol. 137, pp. 310–329, Oct. 2013.

[37] W. B. Cohen, T. K. Maiersperger, Z. Q. Yang, S. T. Gower, D. P. Turner, W. D. Ritts, M. Berterretche, and S. W. Running, "Comparisons of land cover and LAI estimates derived from ETM plus and MODIS for four sites in North America: A quality assessment of 2000/2001 provisional MODIS products," *Remote Sens. Environ.*, vol. 88, no. 3, pp. 233–255, Dec. 2003.

[38] A. Di Gregorio, "Land cover classification system: Classification concepts and user manual for software–version 2," in *Food and Agriculture Organization of the United Nations, Environmental and Natural Resources Series 8*, Rome, Italy, 2005.

[39] E. F. Vermote, N. ElSaleous, C. O. Justice, Y. J. Kaufman, J. L. Privette, L. Remer, J. C. Roger, and D. Tanre, "Atmospheric correction of visible to middle-infrared EOS-MODIS data over land surfaces: Background, operational algorithm and validation," *J. Geophys. Res.*, vol. 102, no. D14, pp. 17131–17141, Jul. 1997.

[40] Y. B. Liu, W. M. Ju, G. L. Zhu, J. M. Chen, B. L. Xing, J. F. Zhu, and Y. L. Zhou, "Retrieval of leaf area index for different grasslands in Inner Mongolia prairie using remote sensing data," (in Chinese) *Acta Ecologica Sinica*, vol. 31, no. 18, pp. 5159–5170, Sep. 2011.

[41] L. Qian and Y. Song, "Analysis of relief amplitude in Liupan mountain based on DEM," (in Chinese) *J. Earth Env.*, vol. 2, no. 4, pp. 510–515, Aug. 2011.

[42] S. Plummer, J. M. Chen, G. Dedieu, and M. Simpson, GLOBCARBON Expert Support Laboratory Input and Output Definition, 1.0 ed., ESRIN, European Space Agency. GLBC/ESL/IODD, Frascati, Italy, 2002.

[43] J. M. Chen and S. G. Leblanc, "Multiple-scattering scheme useful for hyperspectral geometrical optical modelling," *IEEE Trans. Geosci. Remote Sens.*, vol. 39, no. 5, pp. 1061–1071, May 2001.
[44] L. J. Brown, J. M. Chen, S. G. Leblanc, and J. Cihlar, "Short wave infrared correction to the simple ratio: An image and model analysis," *Remote Sens. Environ.*, vol. 71, no. 1, pp. 16–25, 2000.
[45] C. J. Willmott, "On the validation of models," *Phys. Geogr.*, vol. 2, pp. 184–194, 1981.
[46] M. Huang and J. Ji, "The spatial-temporal distribution of leaf area index in China: A comparison between ecosystem modeling and remote sensing reversion," *Acta Ecologica Sinica*, vol. 30, no. 11, pp. 3057–3064, 2010.

Lin Zhu received the M.S. degree from Nankai University, Tianjin, China, in 2005 and the Ph.D. degree in Cartography and GIS from Peking University, Beijing, China. From 2007 to 2008, she was a visiting student with the University of Toronto, Toronto, ON, Canada.

She is currently an Associate Professor with the Meteorological Research Institute of the National Satellite Meteorological Center of the China Meteorological Administration. Her current research interests include the retrieval theory of land surface parameters and the related application research.

Jing M. Chen received the B.Sc. degree in applied meteorology from the Nanjing Institute of Meteorology, Nanjing, China, in 1982, and the Ph.D. degree in meteorology from Reading University, Reading, U.K., in 1986.

He was a Postdoctoral Fellow and Research Associate with the University of British Columbia, Vancouver, BC, Canada, from 1989 to 1993. From 1993 to 2000, he was a Research Scientist with the Canada Centre for Remote Sensing, Ottawa, ON, Canada. He is currently a Professor with the University of Toronto, Toronto, ON, Canada, and an Adjunct Professor with York University, Toronto. He has authored over 200 papers in refereed journals. His current research interests include the remote sensing of biophysical parameters, plant canopy radiation modeling, terrestrial water and carbon cycle modeling, and atmospheric inverse modeling for global and regional carbon budget estimation.

Dr. Chen is a Fellow of the Royal Society of Canada and a Senior Canada Research Chair. He served as an Associate Editor of the IEEE TRANSACTIONS ON GEOSCIENCE AND REMOTE SENSING from 1996 to 2002.

Shihao Tang received the M.S. degree from Nanjing Institute of Meteorology, Nanjing, China, in 1996 and the Ph.D. degree in remote sensing and GIS from Beijing Normal University.

He was a Postdoctoral associates with the Beijing Normal University, Beijing, China, from 2001 to 2003. From 2003 to 2004, he was a visiting scholar with the University of Toronto, Toronto, ON, Canada. He is currently a Professor and vice director with Meteorological research institute of National satellite meteorological center of China Meteorological Administration. His current research interests include the inversion theory of quantitative remote sensing, remote sensing product generation algorithm, and application research.

Dr. Tang is a Fellow of Satellite Meteorology Committee of China Meteorological Society and Committee of Ecological and Agricultural Meteorology.

Guicai Li received the Ph.D. degrees in Cartography and GIS from the Institute of Remote Sensing Applications, Chinese Academy of Sciences (CAS), in 2004.

He was an Assistant Professor in the National Satellite Meteorological Center (NSMC), China Meteorological Administrator (CMA) from 2004 to 2006. Since November 2006, he has been an Associate Professor in NSMC/CMA. He is an author of more than 30 articles. His research interests include the remote sensing inversion of vegetation parameters, ecosystem simulation, and carbon cycles. Dr. Li mainly worked in the algorithm developing and the product validation for satellite land surface product. He is the Chief designer of Large Experiment System (LES) of Fenyun-3 currently, in charge of the designing and the conducting of the Large Experiment System (LES), which is consisted by the aircraft experiment, Calibration and Validation. He have built the field observation system for LST validation and other products in Xilinhot, Dunhuang and other sites since 2008. Dr. Li is a member of National Technical Committee 540 on Climate and Climate Change of Standardization Administration of China (SAC/TC540). He also is a member of the Work Group for Layout Designing and Optimizing of China Meteorological Stations (LDOS-WG).

Zhaodi Guo received the B.S. degree in environmental sciences from Peking University, Beijing, China, in 2005, and the Ph.D. degree in physical geography from Peking University, Beijing, China, in 2011.

Since 2011, she has been an Assistant Research Scientist with the National Satellite Meteorological Center, Beijing, China. Her current research interests include carbon stocks estimation and carbon sinks analysis.

Inter-Comparison and Validation of the FY-3A/MERSI LAI Product Over Mainland China

Lin Zhu, Jing M. Chen, Shihao Tang, Guicai Li, and Zhaodi Guo

***Abstract*—Leaf area index (LAI) is a key surface parameter that describes the structure of vegetation and plays an important role in Earth system process modeling. In this paper, a new set of LAI products (MERSI GLOBCARBON LAI) has been developed based on the GLOBCARBON LAI algorithm and one year of FY-3A/MERSI land surface reflectance data. MERSI GLOBCARBON LAI has been inter-compared and validated over mainland China against MODIS land surface reflectance (LSR) derived LAI (using the same algorithm) and field LAI measurements. MERSI GLOBCARBON LAI and MODIS GLOBCARBON LAI show continuous and smooth LAI distributions at the start and end of the growing season. For most areas in China, the two LAI products agree well. The temporal variation in MERSI GLOBCARBON LAI and MODIS GLOBCARBON LAI consistently follows the growing season. The largest LAI difference occurs during July, when MERSI shows a much higher frequency of retrievals than does MODIS. Through validation of LAI retrievals with field measurements, our study demonstrates that LAI derived from MERSI and MODIS land surface reflectance products have comparable accuracy. MODIS top-of-atmosphere simple ratio (MODIS TOA SR) is related to MERSI TOA SR with linear correlation coefficients greater than 0.6. After atmospheric correction, the correlation coefficient increases from 0.69 to 0.75 over cropland and from 0.82 to 0.93 over grassland. However, atmospheric correction can still give rise to substantial differences in the reflectance data between the two sensors. Furthermore, different land cover types and different terrain relief have contrasting influences on the atmospheric correction, and these influences reduce the agreement between the two LAI products. This study shows the great potential of FY-3A/MERSI data for global LAI retrieval.**

***Index Terms*—FY-3A/MERSI, GLOBCARBON, leaf area index, TERRA/MODIS.**

I. Introduction

REGIONAL and global water and carbon exchange between the land surface and the atmosphere depend greatly on the functioning of plant leaves [1]–[5]. Leaf area index (LAI), defined as half the total leaf area per unit ground surface area [6], is a key vegetation structural parameter of the Earth system used to quantify photosynthesis, respiration, evapotranspiration, canopy interception, energy exchange, and other ecohydrological processes [7]–[9].

Remote sensors with moderate resolution (pixel sizes from 250 m to several kilometers) provide daily and seasonal data at regional and global scales, and these may currently be the best tool to monitor spatial and temporal variations in LAI [10], [11]. Global LAI products have been derived from many remote sensing data sets such as NOAA/AVHRR, TERRA-AQUA/MODIS and SPOT/VEGETATION [12]–[15]. These data sets have provided unprecedented opportunities for studying the Earth's climate [3]. The development of China's new generation of polar-orbiting meteorological satellite series (FY-3) has greatly enhanced surface monitoring [16]. MERSI (Medium Resolution Spectral Imager) is a key multispectral instrument onboard FY-3 satellite [18]. The first two satellites in the series, the morning FY-3A (launched on 27 May 2008) and the afternoon FY-3B (launched on 5 November 2010) provide a 6-hourly revisit capability. This offers the prospect of new, more detailed global LAI products based on this data source. Recently, FY-3A/MERSI LAI Version 1 (MERSI GLOBCARBON LAI), an FY-3A test product from the National Satellite Meteorological Center of China (NSMC), was developed using the GLOBCARBON LAI algorithm [10], [14], [3] and one year of FY-3A/MERSI data. As many other global LAI maps are regularly produced, the accuracy assessment and validation of FY-3A/MERSI LAI are of key importance for potential users.

The overall quality of LAI products depends on several key factors that influence the accuracy of the final retrievals [4]. Uncertainty in input surface reflectance is one of the most important error sources [19], [4], [20]. Surface reflectance time series measured from spaceborne instruments, such as MOderate Resolution Imaging Spectroradiometer (MODIS), show apparent high-frequency noise that limits their information content [21]. The accuracy of surface reflectance products is most affected by the retrieval accuracy of aerosol optical thickness, the Lambertian surface approximation, topography, and viewing-illumination geometry effects [20], [11], [22], [21]. Although different land surface reflectance (LSR) products, such as MODIS surface reflectance collection C5 [23], VGT [24], and MERSI [17], all reduce the uncertainty in the atmospheric correction process using different approaches, the remaining uncertainty may still be considerable. Therefore, as the first step in validating and assessing the FY-3A/MERSI global product, it is desirable to compare the spatial performance of MERSI LSR and MODIS LSR products for LAI retrieval and to evaluate the consistency of LAI time series from different LSR products.

Manuscript received November 18, 2012; revised February 28, 2013; accepted August 19, 2013. This work was supported by the National Basic Research Program of China (Grant 2010CB950700), and China's Research and Development Special Fund for Public Welfare Industry (Meteorology GYHY200906022-1 and Meteorology GYHY200906029). *(Corresponding author: L. Zhu.)*

L. Zhu, S. Tang, G. Li, and Z. Guo are with the National Satellite Meteorological Center of China Meteorological Administration, Beijing, China (e-mail: zhulin@cma.gov.cn; tangsh@cma.gov.cn; ligc@cma.gov.cn; guozd@cma.gov.cn).

J. M. Chen is with the Department of Geography, University of Toronto, Toronto, Ontario, Canada (e-mail: chenj@geog.utoronto.ca).

Color versions of one or more of the figures in this paper are available online at http://ieeexplore.ieee.org.

Digital Object Identifier 10.1109/JSTARS.2013.2280466

The second source of uncertainty arises from misclassifications in the land cover map. Mixed pixel effects can further contribute to errors in land cover classification and introduce extra scaling bias, particularly in moderate-resolution remote sensing data [25], [26]. Pisek and Chen [4] demonstrated that differences in land cover classification for low-resolution images can lead to a difference of $\mathrm{LAI} > 2$ (38%) over the Bigfoot site (Northern Old Black Spruce, Manitoba, Canada) in the middle of boreal summer. Myneni *et al.* [13] estimated that classification errors in land cover maps can generate an LAI estimation error of up to 50%.

The third source of uncertainty is related to the different LAI algorithms used in LAI retrieval. Generally, two kinds of methods are applied to estimate LAI using remote sensing data; i.e., statistical methods [27]–[29], and inversion of physical models [13], [14]. Differences in vegetation structure, land cover, background reflectance, and local topography representation in the LAI algorithms will lead to substantial discrepancies in the final LAI retrievals [11], [30]–[32]. Previous inter-comparisons have shown that GLOBCARBON gives reliable and consistent seasonal and interannual variations [11], and agrees well with Landsat/ETM^{+} LAI maps at most test sites [4], [33]–[35]. Pisek and Chen [4] reported that the median relative absolute error of GLOBCARBON retrievals varied from 24% to 75% at the 1-km scale, compared with 34%–88% for MODIS standard LAI. However, GLOBCARBON tends to underestimate LAI over cropland and grassland, and can exhibit temporal instability during the growing season over evergreen forest sites [36], [11]. The first version of the GLOBCARBON LAI product has also been shown to perform poorly in mountainous areas; the second version includes improvements based on pixel-by-pixel consideration of local topography, clumping index, and background reflectance variations [32].

As the GLOBCARBON LAI algorithm has been validated and evaluated in several comprehensive studies in Canada, China, and other regions, we focus on its use with the new reflectance dataset from FY-3A/MERSI. We perform further inter-comparison, validation, and analysis of the uncertainties in MERSI GLOBCARBON LAI retrieval using both MODIS LSR-derived LAI using the same algorithm (MODIS GLOBCARBON LAI) and field LAI measurements. A case study was conducted over mainland China with the following objectives: (1) to compare the spatial and temporal performance of LAI retrievals from MERSI and MODIS LSR products using GLOBCARBON, (2) to validate and inter-compare MERSI GLOBCARBON LAI with field LAI measurements and other LAI products, and (3) to compare the two LSR data sets and the corresponding level 1 data (TOA reflectance) and further discuss the effect of the uncertainty in MERSI LSR data on LAI estimation.

II. Data

A. Data for LAI Retrieval

1) MERSI Land Surface Reflectance Data: FY-3A/MERSI LSR data for 2010 were downloaded from the National Satellite Meteorological center of China (NSMC) for FY-3A/MERSI LAI retrieval. It has 5 channels with 250 m spatial resolution and 15 channels with 1-km resolution. MERSI LSR is obtained from channels 1–4 of the MERSI 1B product after correction for gaseous absorption, Rayleigh and aerosol scattering, as well as interactions between these processes. Radiative transfer model simulations are used to establish look-up tables (LUTs). Parameters used in the atmospheric correction are interpolated from the pre-established LUTs [17] to achieve a pixel-by-pixel atmospheric correction. Ten-day composites were generated from daily MERSI LSR data for LAI retrieval.

2) MODIS Land Surface Reflectance Data: As the MODIS is one of the most frequently used sensors for LAI retrieval [37], [19], [11], we have chosen MODIS 8-day synthesis surface reflectance products (MOD09) for comparison with and evaluation of the FY-3A/MERSI LAI product. MOD09 corrects for the effects of atmospheric gases, aerosols, and thin cirrus clouds, and is an estimate of the land surface spectral reflectance [23]. MOD09A1 data with 500 m spatial resolution downloaded from NASA's Earth Observing System Data and Information System (EOSDIS) for 2010 were re-projected to geographic latitude/longitude and re-sampled to 1-km resolution for LAI retrieval.

3) Land Cover Data: A land cover map downloaded from the Global Land Cover 2000 database (GLC-2000) is used as an input for LAI retrieval. The GLC-2000 map uses 22 classes based on the Food and Agriculture Organization of the United Nations' hierarchical Land Cover Classification System [38]. This land cover product was adapted for use in the GLOBCARBON LAI algorithm. Some of the cover types with similar structural characteristics were combined, and snow and water body classes were ignored [14].

The spatial agreement of MERSI and MODIS GLOBCARBON LAI was investigated over mainland China and four test sites were selected with different land cover types to further compare the temporal variations of LAI (Fig. 1(a)). These sites are DBF (deciduous broadleaf forest area in the northeast of China, centered at 51.79°N, 121.06°E), DNF (deciduous needleleaf forest area in the northeast of China, centered at 51.78°N, 121.08°E), GLX (grassland in the Xilin Gol prairie of China, centered at 44.14°N, 116.29°E), and CLS (cropland in Yucheng, Shandong province of China, centered at 39.13°N, 115.67°E).

B. Data for Validation

Field LAI measurements were collected in a typical meadow grassland in the Hulunbeier prairie in China (centered at 49.41°N, 119.99°E) during June 21–26, 2010 [40]. Fifty-two 50×50 m sample plots, which have LAI values of 0.46 to 3.08, with a mean value of 1.74 and a standard deviation of 0.61, were set up (Fig. 1(b)). These sample plots are located in homogeneous locations with areas larger than 100×100 m so as to reduce the impact of topography and inhomogeneous land surface. In the center of each sample plot, two observation lines, parallel to the sun line and 25 m apart, were defined, and LAI data were collected using the LAI 2000 instrument along these lines (Fig. 1(c)). This sampling method resulted in 12 LAI measurements for each sample plot, which were then averaged to give the final LAI value for the specified sample plot.

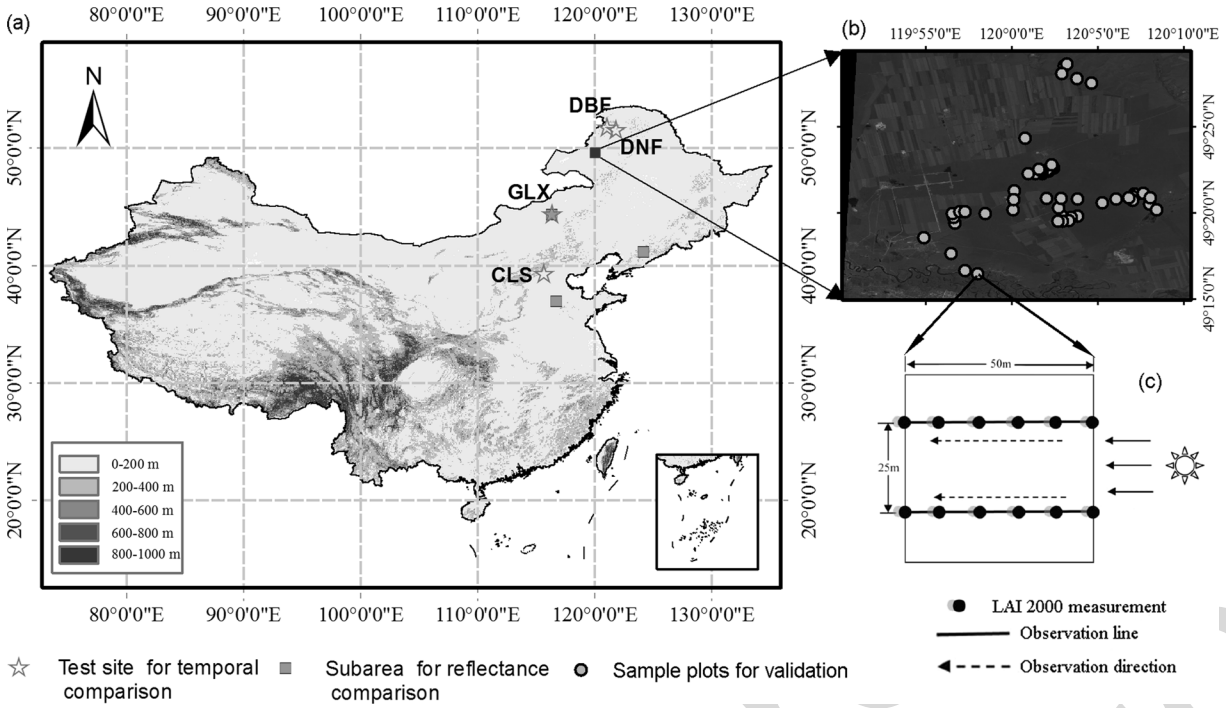

Fig. 1. (a) Map of the relief amplitude over the study area and locations of subarea and test sites for reflectance and temporal comparisons. (b) Locations of field LAI sample plots in a 30-m resolution false color composite map based on TM data. (c) Arrangement of LAI point measurements in a sample plot [40].

TABLE I
DATA SOURCES FOR FIELD VALIDATION AND INTER-COMPARISON OF DIFFERENT LAI PRODUCTS

Dataset name	*Date (Day of year, 2010)*	*Sensor used*	*Product used*	**LAI algorithm**
LAI_{MERSI}	169–176	FY-3A-MERSI	LSR	GLOBCARBON, an inversion model based on the 4-scale geometric optical model (Chen et al., 2002; Deng et al., 2006)
$LAI_{MOD09A1}$	169–176	Terra-MODIS	LSR (MOD09A1)	same as above
$LAI_{MOD15A2}$	169–176	Terra-MODIS	LSR (MOD15A21)	Main algorithm: an inversion model based on a three-dimensional canopy radiative transfer model (Myneni et al., 2002). Backup algorithm: biome-specific relations between NDVI and LAI.
LAI_{TM}	172	Landsat-5 TM	LSR	Site-specific empirical transfer function based on field LAI measurements over Hulunbeier prairie of China (Liu et al., 2011)

A satellite overpass scene (Landsat-5 TM) from 21 June 2010 was selected as the temporally closest cloud-free match to the field measurements (21–26 June 2010). The Landsat-5 TM image was downloaded from the United States Geological Survey (USGS) and converted to TOA radiance using the metadata provided in the TM data header. An atmospheric correction code (6S) [39] was used to convert TOA radiance to land surface reflectance. A vegetation index, Simple Ratio (SR; calculated from Landsat-5 TM data after atmospheric correction) was then correlated with field LAI measurements using an empirical linear function ($R^2 = 0.604$, $RMSE = 0.505$) [40].

To broaden the evaluation of FY-3A/MERSI LAI products, two other LAI products derived from MODIS 8-day synthesis data (MOD09A1 & MOD15A2) were also evaluated. Table I lists the data sources and algorithms for FY-3A/MERSI LAI validation and inter-comparison. All LAI products are re-sampled to 3-km resolution so as to further reduce the influence of image geolocation errors. There are 282 points in total, randomly selected around the LAI field measurement site, and scatter plots were generated to demonstrate the correlation between each pair of LAI products.

C. Data for Uncertainty Analysis

1) Reflectance Data: Four types of remote sensing data were used for the inter-comparison of spectral reflectance between sensors: (a) the MODIS level 1B TOA reflectance product, (b) the corresponding daily LSR products (MYD09GA) downloaded from EOSDIS, (c) the contemporaneous MERSI level

TABLE II
DATA USED FOR REFLECTANCE COMPARISON

Sensor type	Product type	Acquisition dates	Longitude	Latitude	Land cover type
FY-3A/MERSI	Daily TOA reflectance	5-Jun-10	123.84–124.33 °E	40.38–40.88 °N	Broadleaf forest
FY-3A/MERSI	Daily LSR reflectance	5-Jun-10	123.84–124.33 °E	40.38–40.88 °N	
Terra/MODIS	TOA reflectance	5-Jun-10	123.84–124.33 °E	40.38–40.88 °N	
FY-3A/MERSI	Daily TOA reflectance	26-Jun-10	116.08–116.58 °E	44.39–44.44 °N	Grassland
FY-3A/MERSI	Daily LSR reflectance	26-Jun-10	116.08–116.58 °E	44.39–44.44 °N	
Terra/MODIS	TOA reflectance	26-Jun-10	116.08–116.58 °E	44.39–44.44 °N	
Terra/MODIS	LSR reflectance (MYD09GA)	26-Jun-10	116.08–116.58 °E	44.39–44.44 °N	
FY-3A/MERSI	Daily TOA reflectance	25-May-10	116.38–116.91 °E	37.23–37.79 °N	Cropland
FY-3A/MERSI	Daily LSR reflectance	25-May-10	116.38–116.91 °E	37.23–37.79 °N	
Terra/MODIS	TOA reflectance	25-May-10	116.38–116.91 °E	37.23–37.79 °N	
Terra/MODIS	LSR reflectance (MYD09GA)	25-May-10	116.38–116.91 °E	37.23–37.79 °N	

1B TOA reflectance, and (d) the corresponding daily LSR products with 1-km resolution distributed by NSMC. MERSI and MODIS TOA and LSR products were all co-registered and aggregated to 1-km resolution.

MERSI and MODIS 1B and LSR products were chosen over three typical areas with adjacent overpass times, small zenith view angles, and cloud-free conditions. The acquisition dates, position, land cover types, and observation geometry for the selected MERSI and MODIS TOA reflectance and LSR images are given in Table II.

D. Topographic Data

A relief amplitude map (Fig. 1(a)) of the study area is used to describe quantitatively the influence of topographic characteristics on LAI retrieval. The map was generated using a digital elevation model (DEM; SRTM 4.1, Shuttle Radar Topography Mission) and the neighborhood statistics function of ArcGIS [41]. Relief amplitude is defined as the vertical difference in elevation between the highest and lowest points for a particular area (3×3 pixels, with 1-km resolution), and is used to quantify the localized changes in terrain across the landscape. As shown in Fig. 1(a), the relief amplitude in most of the study area is less than 400 m. However, in southwest China, the relief amplitude increases up to 1000 m, indicating large slopes in this area.

III. METHOD

A. GLOBCARBON LAI Algorithm

The European Space Agency funded GLOBCARBON, an initiative to produce multi-year global Level 3 land products that include LAI [42], for the purpose of global carbon cycle modeling [3]. Products derived from data from the VEGETATION instrument, the Along Track Scanning Radiometers (AATSR and ATSR-2), and the Medium Resolution Imaging Spectrometer (MERIS) are available for the period 1998–2007. GLOBCARBON uses a geometric optical model (Four-Scale model) [30] with a multiple scattering scheme [43] and LAI algorithms previously derived for Canada-wide applications [10] to establish angle-specific relationships between Simple Ratio (SR) and LAI, and between Reduced SR (RSR) and LAI for various land cover types [14].

SR and RSR are the starting points for LAI retrieval and can be expressed as

$$\mathrm{SR} = \frac{\rho_{\mathrm{NIR}}}{\rho_{\mathrm{Red}}} \tag{1}$$

where ρ_{NIR} and ρ_{Red} are the reflectances in the near infrared and red bands, respectively.

RSR is defined as

$$\mathrm{RSR} = \frac{\rho_{\mathrm{NIR}}}{\rho_{\mathrm{Red}}} \left(1 - \frac{\rho_{SWIR} - \rho_{SWIR_{\min}}}{\rho_{SWIR_{\max}} - \rho_{SWIR_{\min}}}\right) \tag{2}$$

where ρ_{SWIR} is the reflectance in the SWIR band and $\rho_{SWIR_{\max}}$ and $\rho_{SWIR_{\min}}$ are the maximum and minimum SWIR reflectances for specific land covers, respectively [44], [14].

Bidirectional reflectance distribution function (BRDF), land cover, foliage clumping, and soil background effects are all explicitly considered in GLOBCARBON algorithm through Four-Scale model simulations. Relationships between SR and LAI over large ranges of viewing and illumination angles and land cover types can be expressed as

$$\mathrm{LAI} = f_{L\_SR}(\mathrm{SR} \cdot f_{BRDF}(\theta_v, \theta_s, \varphi)) \tag{3}$$

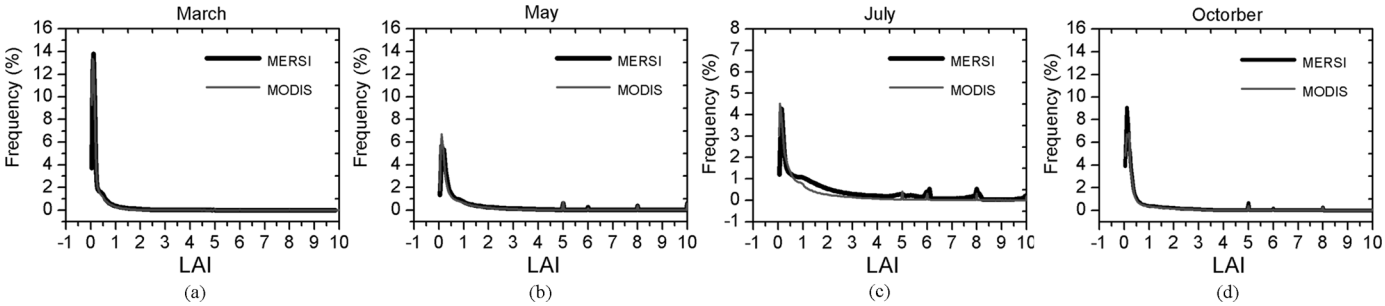

Fig. 2. Comparison of LAI value distribution over China for (a) March, (b) May, (c) July, and (d) October of 2010.

where θ_s is the solar zenith angle (SZA), θ_v is the view zenith angle (VZA), φ is the relative azimuth angle, $f_{BRDF}()$ is the BRDF modification function for SR, and $f_{L\_SR}()$ is a function describing the relationship between BRDF-modified SR and LAI.

Similarly, LAI–RSR relationships have been established as follows [14]

$$\mathrm{LAI} = f_{L\_RSR}\left(\mathrm{SR}\cdot f_{BRDF}(\theta_v,\theta_s,\varphi) \cdot\left(1-\frac{\rho_{SWIR}\cdot f_{SWIR\_BRDF}(\theta_v,\theta_s,\varphi)-\rho_{\mathrm{SWIRmin}}}{\rho_{\mathrm{SWIRmax}}-\rho_{\mathrm{SWIRmin}}}\right)\right) \tag{4}$$

where $f_{L\_RSR}()$ is a function describing the relationship between BRDF-modified RSR and LAI, and $f_{SWIR\_BRDF}()$ is a BRDF modification function for SWIR reflectance. The use of the SWIR band in RSR gives LAI-RSR relationships that minimize the variable background effect on LAI retrieval over forest [14].

To further minimize residual atmospheric effects, GLOBCARBON uses a procedure known as Locally Adjusted Cubic-spline Capping (LACC) [3] to reconstruct the seasonal trajectory of LAI. In LACC, a variable local smoothing parameter is automatically determined according to the local curvature of the original seasonal variation pattern. The final optimal solution is obtained from an iteration procedure by progressively replacing anomalously low values with fitted values [3].

B. Spatial Agreement Analysis Method

The spatial agreement of MERSI GLOBCARBON LAI and MODIS GLOBCARBON LAI is evaluated using an agreement index [45] defined as

$$A_{index} = 1 - \frac{\sum_{k=1}^{n}(P_k - O_k)^2}{\sum_{k=1}^{n}\left[(|P'_k| + |O'_k|)^2\right]} \tag{5}$$

where $P'_k = P_k - \overline{O}$ and $O'_k = O_k - \overline{O}$, O are observations, P are model predictions, $\overline{O}$ represents the observed mean, and n is the number of matching pairs over the study period. The agreement index (A_{index}) ranges from 0 to 1; i.e., from no agreement to perfect agreement between observation and prediction. In the present study, O represents MERSI GLOBCARBON LAI and P represents MODIS GLOBCARBON LAI at the same location and same time, and $n = 5$ matching pairs in 2010 (8-day synthesis LAI retrievals: 9–10 January, 22–30 March, 17–24 May, 20–27 July, and 24–31 October).

IV. Results and Discussion

A. Comparison of MERSI and MODIS GLOBCARBON LAI

1) Spatial Frequency: Fig. 2(a)–(d) displays the LAI histograms for MERSI GLOBCARBON LAI and MODIS GLOBCARBON LAI in four specific months (March, May, July, and October 2010) that cover the main vegetation growing period. Frequency is given as a percentage of the total number of pixels over mainland China.

Both MERSI GLOBCARBON LAI and MODIS GLOBCARBON LAI show continuous and smooth frequency distributions in March (as shown in Fig. 2(a)). MODIS has a higher frequency of retrievals at low LAI values (LAI less than 0.04). During May and October, these two LAI products also show continuous smooth frequency patterns except for several small peaks at LAI values 5, 6, and 8, which are artifacts associated with the maximum LAI limits in the GLOBCARBON LAI algorithm for different land cover types. The largest LAI differences between these two products occur at the peak of the growing season during July (Fig. 2(c)), when MERSI shows a much higher frequency of retrievals with LAI greater than 0.75 than does MODIS. For both LAI products, the frequency of low LAI values is very high at the start and end of the growing season, and decreases during the peak growing season, which is consistent with other LAI products and is in agreement with vegetation growth over northern latitudes [11].

2) Spatial Agreement: The spatial performance of the MERSI and MODIS retrievals using the GLOBCARBON algorithm over mainland China from January to October 2010 is shown in Fig. 3. The agreement index is larger than 0.8 (0.6) for 38.85% (63.17%) of the land area in mainland China, suggesting that in most locations, LAI retrievals from MERSI and MODIS agree well. However, some low values of agreement index are found in southeast China due to frequent cloud cover that influences MERSI and MODIS reflectance differently.

3) Temporal Variations: The temporal variations of MERSI GLOBCARBON LAI and MODIS GLOBCARBON LAI over four test sites (Fig. 1) with different land cover types were compared for a full year in 2010. As shown in Fig. 4(a), over DBF, MERSI GLOBCARBON LAI and MODIS GLOBCARBON LAI have similar trends, especially during the growing season,

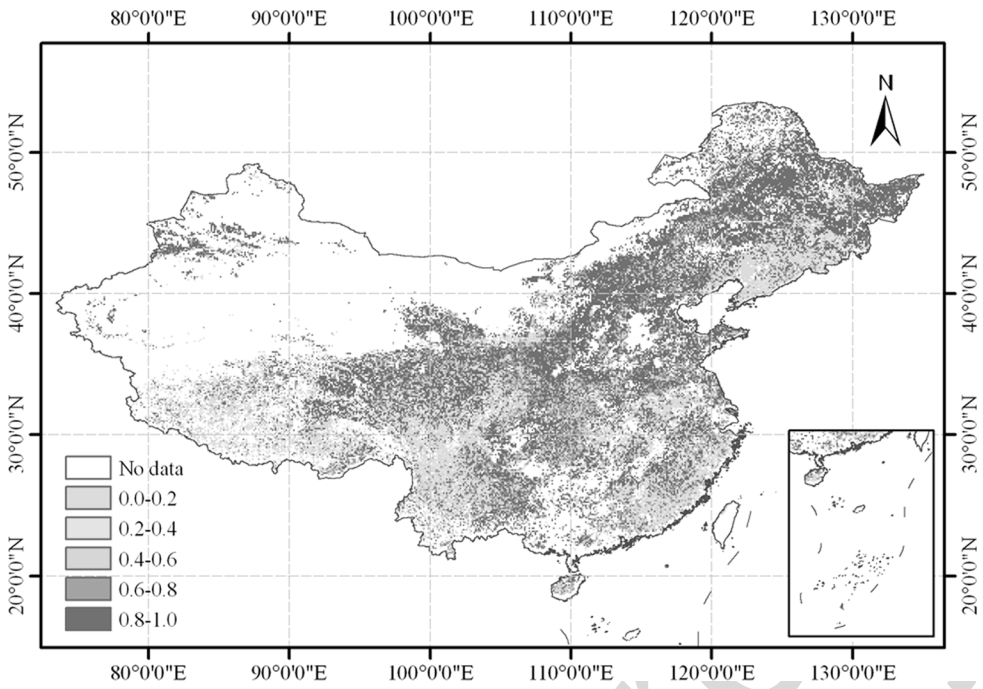

Fig. 3. Agreement index between MERSI GLOBCARBON LAI and MODIS GLOBCARBON LAI using 5 matching pairs of 8-day synthesis LAI retrievals in 2010 (9–10 January, 22–30 March, 17–24 May, 20–27 July and 24–31 October).

but their magnitudes differ during the peak growing season. At the end of the growing season, MERSI GLOBCARBON LAI decreases earlier than MODIS GLOBCARBON LAI. It is also obvious that there are several anomalously low LAI values in MODIS and MERSI LAI trajectories due to the remaining effects of cloud and aerosol on multi-day composite reflectance data. We can also see the improvement in MERSI GLOBCARBON LAI after applying LACC smoothing. Erratic LAI values in MERSI GLOBCARBON LAI trajectories were corrected, giving a smoother seasonal variation of LAI that better resembles the expected variation in vegetation growth. At the peak of the growing season, there are distinct differences between MERSI GLOBCARBON LAI and MODIS GLOBCARBON LAI. An earlier study has shown that the maximum LAI for broadleaf forest is 4–6 in northeast China [46]. For broadleaf forests, MERSI GLOBCARBON LAI is larger than MODIS GLOBCARBON LAI.

Over DNF (Fig. 4(b)), MODIS and MERSI GLOBCARBON LAI retrievals are similar but both seem to overestimate LAI. Considering that the same LAI algorithm was used for MERSI and MODIS, the biases of these LAI products may be caused by uncertainties in the atmospheric correction process and the difference in spectral response functions between the two sensors. For dense canopies in particular, near infrared reflectance saturates at moderate LAI values (2–4), and a very small bias in the red band reflectance due to error in atmospheric correction will lead to a significant bias in vegetation index, which tends to destabilize the LAI retrieval [11].

Over GLX (Fig. 4(c)), MERSI GLOBCARBON LAI and MODIS GLOBCARBON LAI follow the beginning and the end of the season reasonably well, but from day of year 120, MODIS GLOBCARBON LAI begins to diverge from MERSI GLOBCARBON LAI. During the peak growing season, MODIS GLOBCARBON LAI is lower than MERSI GLOBCARBON LAI. The typical LAI value for GLX in the same area is 1–3 from ecosystem model simulation and field LAI observations [36]. Considering the mixed pixel effect from field scale to regional scale, the actual LAI retrieved from moderate resolution remote sensing data is expected to be lower.

Over CLS (Fig. 4(d)), both MERSI GLOBCARBON LAI and MODIS GLOBCARBON LAI display a two-peak pattern, which is a fair representation of the succession between winter wheat and summer corn. During the peak of winter wheat growth, MERSI GLOBCARBON LAI is a little higher than MODIS GLOBCARBON LAI, whereas during the peak of summer corn growth, MODIS GLOBCARBON LAI attains an anomalously high value, which is possibly related to the erratic land surface reflectance due to the remaining atmospheric effects. The start and end of the growing season for MODIS GLOBCARBON LAI do not coincide with those for MERSI GLOBCARBON LAI. This is possibly due to different composite periods for the two LAI products. MERSI GLOBCARBON LAI is computed from 10-day composites of MERSI LSR images using the maximum normalized difference vegetation index (NDVI) criterion, whereas MODIS GLOBCARBON LAI was calculated from 8-day cloud-free composites of MODIS LSR images.

B. Validation

Fig. 5(a)–(c) compares LAI derived from moderate resolution sensors including MERSI and MODIS with measured LAI aggregated to 3-km resolution using TM data ($\mathrm{LAI_{TM}}$). Although the different LAI data generally vary in a similar fashion, the scatter of data points is considerable (SD ranges from 0.36 to 0.51). In Fig. 5(a) and (b), even though the same LAI algorithm was used for $\mathrm{LAI_{MERSI}}$ and $\mathrm{LAI_{MOD09A1}}$, uncertainties in the

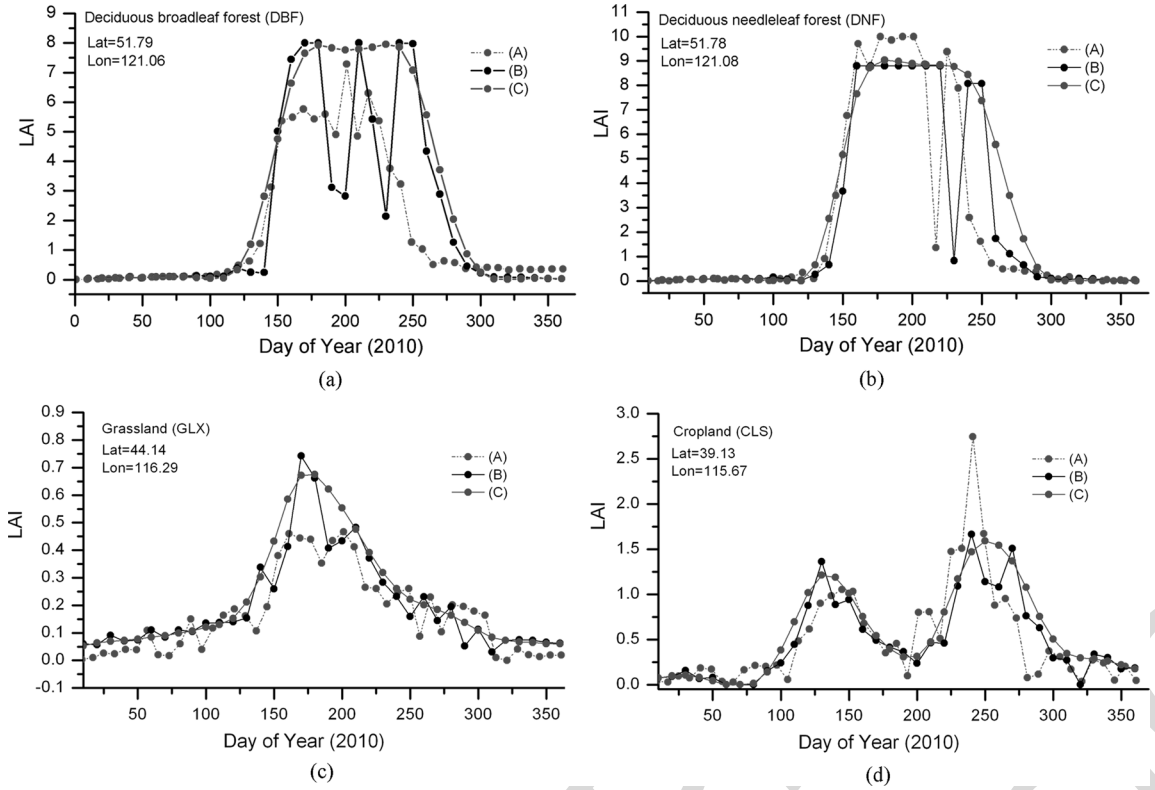

Fig. 4. Seasonal variations in MERSI GLOBCARBON LAI and MODIS GLOBCARBON LAI for (a) deciduous broadleaf forest, (b) deciduous needleleaf forest, (c) grassland, and (d) cropland. (A) Red dots represent MODIS GLOBCARBON LAI without LACC smoothing, (B) black dots represent MERSI GLOBCARBON LAI without LACC smoothing, and (C) green dots represent MERSI GLOBCARBON LAI with LACC smoothing.

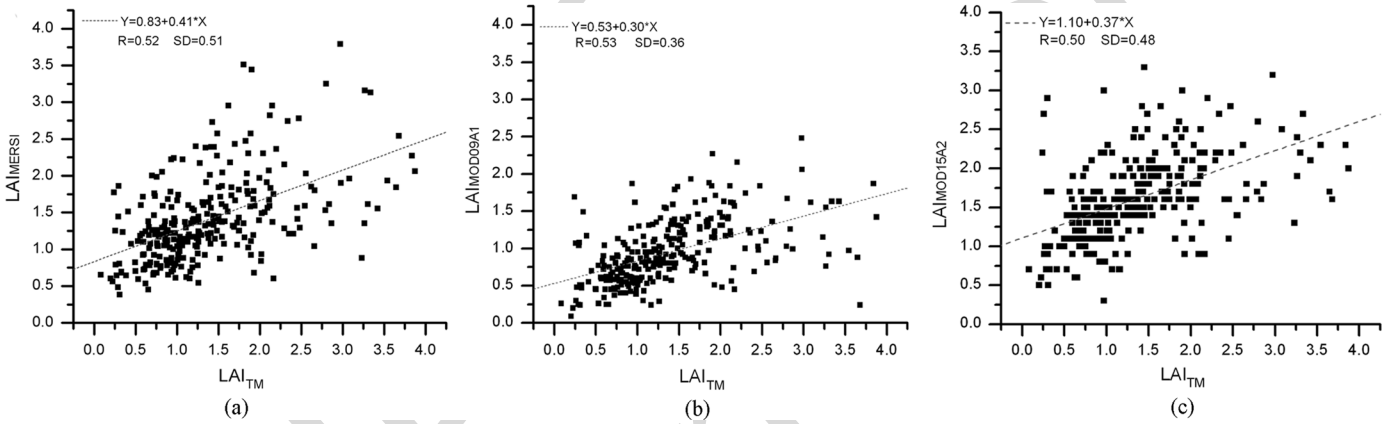

Fig. 5. Inter-comparison and validation of MERSI LAI and other LAI products: (a) MERSI GLOBCARBON LAI vs. TM LAI, (b) MODIS GLOBCARBON LAI vs. TM LAI, and (c) MODIS standard LAI product vs. TM LAI.

atmospheric correction process for MERSI and MODIS images possibly contribute to the large differences between the final LAI retrievals. The slight difference between $LAI_{MOD09A1}$ and $LAI_{MOD15A21}$ performance compared with LAI_{TM}, however, can be attributed to the different LAI algorithms used in LAI retrieval. The correlation coefficient R varies slightly from 0.50 to 0.53 in Fig. 5(a) to (c), suggesting that the three LAI products (i.e., LAI_{MERSI}, $LAI_{MOD09A1}$ and $LAI_{MOD15A21}$), which use two different LAI algorithms and data from two different sensors, have comparable accuracy relative to the high resolution aggregated LAI (LAI_{TM}) over grassland.

C. Uncertainty Analysis

1) Influence of Input Reflectance: Vegetation indices (SR or RSR) derived from red, near infrared, and shortwave infrared reflectance are the starting point for LAI calculation with the GLOBCARBON LAI algorithm. SR is more sensitive to atmospheric conditions than is RSR. The influence of the atmospheric correction procedure on the final accuracy of LAI was investigated further using scatter plots between MODIS and MERSI TOA-reflectance-derived SR and LSR-derived SR for three typical areas of China with different land cover types.

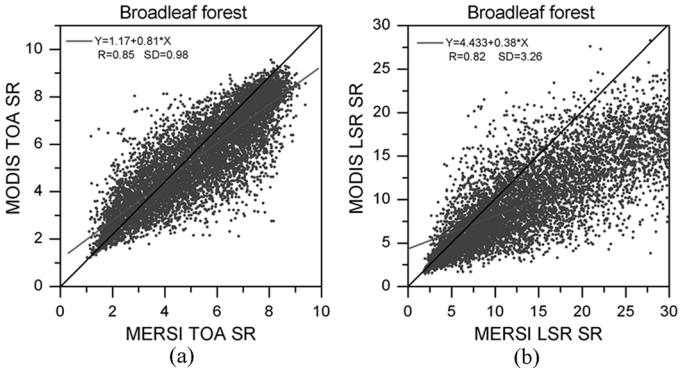

Fig. 6. Scatter plot between MERSI and MODIS data over broadleaf forest area for (a) TOA reflectance and (b) LSR.

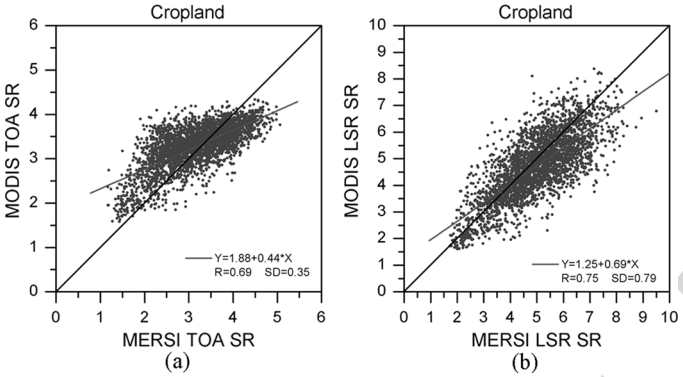

Fig. 7. Scatter plot between MERSI and MODIS data over cropland for (a) TOA reflectance and (b) LSR.

It is encouraging that MODIS TOA SR and MERSI TOA SR are well correlated for all three land cover types, with linear correlation coefficients higher than 0.6 (as shown in Figs. 6–8). The lowest correlation coefficient (R) of up to 0.69 is found over cropland and the maximum R of up to 0.82 is found over grassland, showing the comparable capability and quality of MERSI and MODIS for vegetation monitoring. The regression slope mainly shows differences between MERSI and MODIS due to the spectral response and point spread functions. After atmospheric correction, the relationship between MODIS LSR SR and MERSI LSR SR is slightly better than that between MODIS TOA SR and MERSI TOA SR for grassland and cropland, although by different degrees (R increases from 0.82 to 0.93 over grassland and from 0.69 to 0.75 over cropland), suggesting that using the ratio of the red and NIR spectral bands can effectively reduce the influence of atmospheric contamination.

However, atmospheric correction is still one of the main causes of scatter between data from the two sensors. As shown in Figs. 6–8, for different land cover types, the SD values are all higher after atmospheric correction. The highest SD value is observed over forest (Fig. 6(b)). According to the Four-scale simulations, the shadow effect of forest will reduce the red band reflectance, while strengthening multiple scattering of the NIR band radiation, shifting the saturation of SR signals to higher LAI values [10]. Therefore, while the forest shadow effect makes the final MERSI LAI higher than MODIS LAI

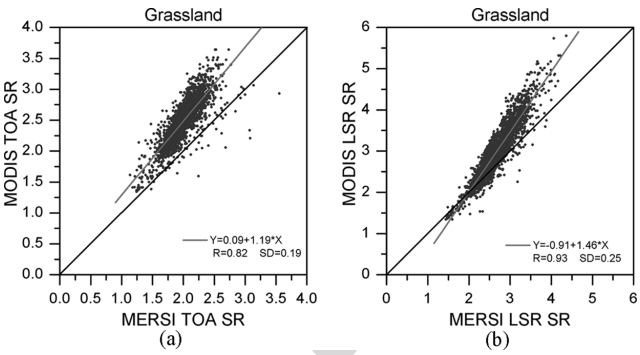

Fig. 8. Scatter plot between MERSI and MODIS data over grassland for (a) TOA reflectance and (b) LSR.

during the peak growing season for broadleaf forests (as shown in Fig. 6(a)–(c)), it also tends to introduce large uncertainty in the red band during atmospheric correction and greatly influences the SR value, increasing the scatter among the data points (Fig. 6(b)).

Apart from atmospheric contamination and land cover, the mixed pixel effect, acquisition time difference, and geo-location are all potential factors causing large scatter around the regression line. As shown in Fig. 6(a), over forest, the data scatter is greatest in the center of the plot, indicating mixed pixels. Over grassland, MODIS SR is generally higher than MERSI. This disagrees with the result of Fig. 4(c) where MERSI LAI is higher than MODIS LAI during the growing season. In Fig. 4, 10-day MERSI LSR composite images and 8-day MODIS LSR composite images are used for comparing the temporal variation, whereas in Fig. 6 only one scene is used. This result reinforces the view that differences in image acquisition date are another major reason for discrepancies between MODIS SR and MERSI SR, as shown in previous studies (e.g., [4]).

2) Influence of Land Cover Type and Topography: The frequency of pixels with agreement index greater than 0.5 for different land cover types and relief amplitude index values are shown in Figs. 9 and 10, respectively. For most land cover types, more than 72% of pixels have an agreement index greater than 0.5, suggesting that MERSI GLOBCARBON LAI and MODIS GLOBCARBON LAI agree well in space and time. Compared with other land cover types, grassland has the highest frequency of high values (> 0.5). This result is consistent with the fact that MERSI SR and MODIS SR have the highest linear correlation coefficient (R) over grassland, as shown in Section IV.C.1. In the case of broadleaf and mixed forest, the greatest disagreement arises from the significant overestimate of SR by MERSI LSR (as shown in Fig. 6(b)), which results in large numbers of upper bound LAI values in the MERSI GLOBCARBON LAI.

The spatial variation of is better correlated with the relief amplitude index (Fig. 10) than with land cover type. As the relief amplitude index increases, the frequency of > 0.5 decreases. Uncertainty in the estimation of surface reflectance is a major contributor to this variation. MODIS and MERSI LSR products all use a Lambertian surface approximation for atmospheric correction instead of a BRDF correction process [23], [17], which will reduce the accuracy of the LSR product, especially in hilly

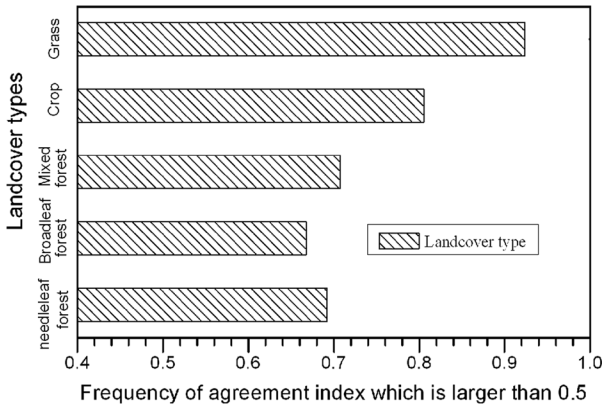

Fig. 9. Frequency of agreement index greater than 0.5 for different land cover types.

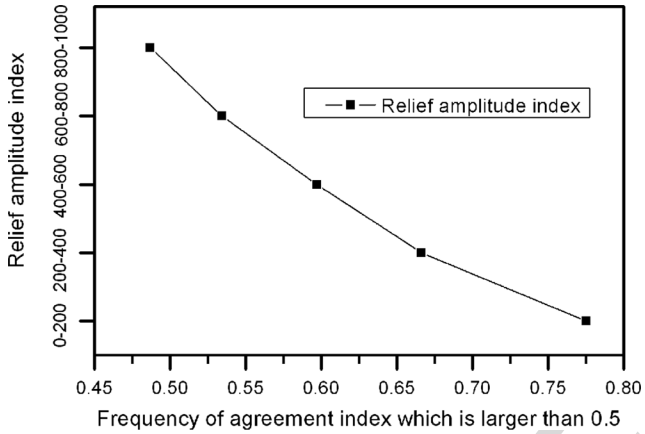

Fig. 10. Frequency of agreement index greater than 0.5 for different relief amplitude indexes.

areas [11]. The complex terrain effect may introduce uncertainties into the atmospheric correction process, and therefore increases the discrepancy between the two LAI products.

V. Summary and Conclusion

In this study, the spatial and temporal performance of the FY-3A/MERSI LSR product for LAI retrieval using the GLOBCARBON LAI algorithm are inter-compared and validated with MODIS LSR derived LAI and field LAI measurements over mainland China. The influence of input reflectance, land cover type, and topography on the final accuracy of LAI are further explored and discussed. The following conclusions are drawn.

a) MERSI GLOBCARBON LAI and MODIS GLOBCARBON LAI show a continuous and smooth LAI distribution at the start and end of the growing season. These two LAI products agree well, with an agreement index greater than 0.5, over 72.08% of mainland China. The largest LAI difference occurs during July, MERSI shows a much higher frequency of retrievals than does MODIS. The overestimate of MERIS GLOBCARBON LAI in the peak growing season is mainly due to the overestimate of SR derived from MERSI-LSR in dense canopies, causing a mismatch between the reflectance modeled by the LAI algorithm and the MERSI derived land surface reflectance.

b) Our study demonstrates that LAI values derived from MERSI LSR and MODIS LSR have comparable accuracy relative to an independent LAI map derived using a Landsat TM image (LAITM) in combination with ground LAI data. Of all the LAI values derived from MERSI and MODIS, MODIS GLOBCARBON LAI has the best correlation with LAITM ($R = 0.53$). This result indicates that the GLOBCARBON LAI algorithm performs slightly better than the standard MODIS LAI algorithm, which is based mainly on a radiative transfer model.

c) There are good relationships between MODIS TOA SR and MERSI TOA SR for all three land cover types, with linear correlation coefficients greater than 0.6. By taking the ratio between the red and NIR spectral bands, SR can effectively reduce the influence of atmospheric contamination. However, atmospheric correction is still a cause of scatter among data from the two sensors.

d) Different land cover types and different terrain relief index values have contrasting influences on the atmospheric correction, and these influences reduce the agreement between MODIS and MERSI GLOBCARBON LAI.

This study focused solely on mainland China, and limited field measurement data were used for LAI product evaluation. Global use of MERSI GLOBCARBON LAI products will require additional validation in other areas. Furthermore, in the Results and Discussion sections, we made a special effort to discuss the uncertainty in the LAI–SR relationship of the GLOBCARBON algorithm. It is also important to show how MERSI and MODIS SWIR reflectance relate to each other since the GLOBCARBON algorithm also relies on SWIR reflectance. We will investigate these considerations in future work. This study shows the great potential of FY-3A/MERSI LAI for global vegetation monitoring and for further effective use in ecosystem modeling.

Acknowledgment

The authors are most grateful to Prof. W. M. Ju and Dr. Y. Liu of Nanjing University, China, for help with field LAI measurement collection and LAI validation, and to two anonymous reviewers for constructive comments that greatly improved the manuscript.

References

[1] G. B. Bonan, "Land-atmospheric interactions for climate system models: Coupling biophysical, biogeochemical and ecosystem dynamical processes," *Remote Sens. Environ.*, vol. 51, no. 1, pp. 57–73, Jan. 1995.

[2] P. J. Sellers, F. G. Hall, R. D. Kelley, A. Black, D. Baldocchi, J. Berry, M. Ryan, K. J. Ranson, P. M. Crill, D. P. Lettenmaier, H. Margolis, J. Cihlar, J. Newcomer, D. Fitzjarrald, P. G. Jarvis, S. T. Gower, D. Halliwell, D. Williams, B. Goodison, D. E. Wickland, and F. E. Guertin, "BOREAS in 1997: Experiment overview, scientific results, and future directions," *J. Geophys. Res.*, vol. 102, no. D24, pp. 28731–28769, Dec. 1997.

[3] J. M. Chen, F. Deng, and M. Chen, "Locally adjusted cubic-spline capping for reconstructing seasonal trajectories of a satellite-derived surface parameter," *IEEE Trans. Geosci. Remote Sens.*, vol. 44, no. 8, pp. 2230–2238, Aug. 2006.

[4] J. Pisek and J. M. Chen, "Comparison and validation of MODIS and VEGETATION global LAI products over four BigFoot sites in North America," *Remote Sens. Environ.*, vol. 109, no. 1, pp. 81–94, Aug. 2007.

[5] N. C. Coops, R. H. Waring, and J. J. Landsberg, "Estimation of potential forest productivity across the Oregon transect using satellite data and monthly weather records," *Int. J. Remote Sens.*, vol. 22, no. 18, pp. 3797–3812, 2001.

[6] J. M. Chen and T. A. Black, "Defining leaf-area index for nonflat leaves," *Plant Cell Environ.*, vol. 15, no. 4, pp. 421–429, May 1992.

[7] M. Weiss, F. Baret, G. Smith, I. Jonckheere, and P. Coppin, "Review of methods for in situ leaf area index (LAI) determination, Part II. Estimation of LAI, errors and sampling," *Agr. Forest Meteorol.*, vol. 121, no. 1–4, pp. 37–53, Jan. 2004.

[8] G. B. Bonan, "Forests and climate change: Forcings, feedbacks, and the climate benefits of forests," *Science*, vol. 320, no. 5882, pp. 1444–1449, Jun. 2008.

[9] Implementation Plan for the Global Observing System for Climate in Support of the UNFCCC, WMO, 2010, GCOS Report No. 138, GOOS Report No. 184 (WMO- TD/No. 1523).

[10] J. M. Chen, G. Pavlic, L. Brown, J. Cihlar, S. G. Leblanc, H. P. White, R. J. Hall, D. R. Peddle, D. J. King, J. A. Trofymow, E. Swift, J. Van der Sanden, and P. K. E. Pellikka, "Derivation and validation of Canada-wide coarse-resolution leaf area index maps using high-resolution satellite imagery and ground measurements," *Remote Sens. Environ.*, vol. 80, no. 1, pp. 165–184, Apr. 2002.

[11] S. Garrigues, R. Lacaze, F. Baret, J. T. Morisette, M. Weiss, J. E. Nickeson, R. Fernandes, S. Plummer, N. V. Shabanov, R. B. Myneni, Y. Knyazikhin, and W. Yang, "Validation and intercomparison of global leaf area index products derived from remote sensing data," *J. Geophys. Res., Biogeosci.*, vol. 113, no. G2, pp. 1–20, Jun. 2008.

[12] P. J. Sellers, S. O. Los, C. J. Tucker, C. O. Justice, D. A. Dazlich, G. J. Collatz, and D. A. Randall, "A revised land surface parameterization (SiB2) for atmospheric GCMS. Part II: The generation of global fields of terrestrial biophysical parameters from satellite data," *J. Clim.*, vol. 9, no. 4, pp. 706–737, Apr. 1996.

[13] R. B. Myneni, Y. Knyazikhin, J. L. Privette, J. Glassy, Y. Tian, Y. Wang, X. Song, Y. Zhang, G. R. Smith, A. Lotsch, M. Friedl, J. T. Moriestte, P. Votava, R. R. Nemani, and S. W. Running, "Global products of vegetation leaf area and fraction absorbed PAR from year one of MODIS data," *Remote Sens. Environ.*, vol. 83, no. 1–2, pp. 214–231, Feb. 2002.

[14] F. Deng, J. M. Chen, S. Plummer, and J. Pisek, "Algorithm for global leaf area index retrieval using satellite imagery," *IEEE Trans. Geosci. Remote Sens.*, vol. 44, no. 8, pp. 2219–2229, Aug. 2006.

[15] F. Baret, O. Hagolle, B. Geiger, P. Bicheron, B. Miras, M. Huc, B. Berthelot, F. Nino, M. Weiss, O. Samain, J. L. Roujean, and M. Leroy, "LAI, fAPAR and fCover CYCLOPES global products derived from VEGETATION, Part 1: Principles of the algorithm," *Remote Sens. Environ.*, vol. 110, no. 3, pp. 275–286, Oct. 2007.

[16] J. Yang, C. H. Dong, N. M. Lu, Z. D. Yang, J. M. Shi, P. Zhang, Y. J. Liu, and B. Cai, "FY-3A: The new generation polar-orbiting meteorological satellite of China," *Acta Meteorologica Sinica*, vol. 67, no. 4, pp. 501–509, Dec. 2009.

[17] J. Yang *et al.*, "MERSI land surface reflectance with 250 m resolution," in *Operational Products and Application of New Generation of FY Polar-Obit Meteorological Satellite*, 1st ed. Beijing, China: Science Press, 2011, pp. 250–252.

[18] C. Dong, J. Yang, W. Zhang, Z. Yang, N. Lu, J. Shi, P. Zhang, Y. Liu, and B. Cai, "An overview of a new Chinese weather satellite FY-3A," *Bull. Amer. Meteorol. Soc.*, vol. 90, no. 10, pp. 1531–1544, Oct. 2009.

[19] B. Tan, J. Hu, D. Huang, W. Yang, P. Zhang, N. V. Shabanov, Y. Knyazikhin, R. R. Nemani, and R. B. Myneni, "Assessment of the broadleaf crops leaf area index product from the Terra MODIS instrument," *Agr. Forest Meteorol.*, vol. 135, no. 1–4, pp. 124–134, Dec. 2005.

[20] Y. Yi, D. Yang, J. Huang, and D. Chen, "Evaluation of MODIS surface reflectance products for wheat leaf area index (LAI) retrieval," *Int. J. Remote Sens.*, vol. 63, no. 6, pp. 661–677, Nov. 2008.

[21] F. M. Bréon and E. Vermote, "Correction of MODIS surface reflectance time series for BRDF effects," *Remote Sens. Environ.*, vol. 125, pp. 1–9, Oct. 2012.

[22] E. Vermote, C. O. Justice, and F. M. Breon, "Towards a generalized approach for correction of the BRDF effect in MODIS directional reflectances," *IEEE Trans. Geosci. Remote Sens.*, vol. 47, no. 3, pp. 898–908, Mar. 2009.

[23] E. F. Vermote and A. Vermeulen, Atmospheric Correction Algorithm: Spectral Reflectances (MOD09), NASA, contract NAS5-96062, 1999 [Online]. Available: http://modis.gsfc.nasa.gov/data/atbd/atbd_mod08.pdf

[24] P. Maisongrande, B. Duchemin, and G. Dedieu, "VEGETATION/SPOT: An operational mission for the Earth monitoring; presentation of new standard products," *Int. J. Remote Sens.*, vol. 25, no. 1, pp. 9–14, Jan. 2004.

[25] J. M. Chen, "Spatial scaling of a remotely sensed surface parameter by contexture," *Remote Sens. Environ.*, vol. 69, no. 1, pp. 30–42, Jul. 1999.

[26] S. Garrigues, D. Allard, and F. Baret, "Influence of the spatial heterogeneity on the nonlinear estimation of Leaf Area Index from moderate resolution remote sensing data," *Remote Sens. Environ.*, vol. 105, no. 4, pp. 286–298, Dec. 2006.

[27] J. W. Rouse, R. H. Haas, J. A. Schell, and D. W. Deering, "Monitoring vegetation systems in the great plains with ERTS," in *Proc. 3rd ERTS Symp.*, 1973, vol. 1, pp. 309–317.

[28] J. M. Chen, "Evaluation of vegetation indices and a modified simple ratio for boreal application," *Can. J. Remote Sens.*, vol. 22, no. 3, pp. 229–242, Jan. 1996.

[29] F. M. Wang, J. F. Huang, Y. L. Tang, and X. Z. Wang, "New vegetation index and its application in estimating leaf area index of rice," *Chin. J. Rice Sci.*, vol. 21, no. 2, pp. 159–166, Sep. 2007.

[30] J. M. Chen and S. G. Leblanc, "A 4-scale bi-directional reflection model based on canopy architecture," *IEEE Trans. Geosci. Remote Sens.*, vol. 35, no. 5, pp. 1316–1337, Sep. 1997.

[31] K. Richter, C. Atzberger, F. Vuolo, and G. D'Urso, "Evaluation of Sentinel-2 spectral sampling for radiative transfer model based LAI estimation of wheat, sugar beet, and maize," *IEEE J. Sel. Topics Appl. Earth Observ. Remote Sens. (JSTARS)*, vol. 4, no. 2, pp. 458–464, Jun. 2011.

[32] A. Gonsamo and J. M. Chen, "Improved LAI algorithm implementation to MODIS data by incorporating background, topography, and foliage clumping information," *IEEE Trans. Geosci. Remote Sens.*, 2013, DOI: 10.1109/TGRS.2013.2247405.

[33] R. Liu, J. M. Chen, J. Liu, F. Deng, and R. Sun, "Application of a new leaf area index algorithm to China's landmass using MODIS data for carbon cycle research," *J. Environ. Manage.*, vol. 85, no. 3, pp. 649–658, Nov. 2007.

[34] X. F. Li, W. M. Ju, Y. L. Zhou, and S. Chen, "Retrieving leaf area index of forests in red soil hilly region using remote sensing data," in *Proc. SPIE 7471*, Oct. 2009.

[35] Y. B. Liu, W. M. Ju, J. M. Chen, G. L. Zhu, B. L. Xing, J. F. Zhu, and M. Z. He, "Spatial and temporal variations of forest LAI in China during 2000–2010," *Chin. Sci. Bull.*, vol. 57, no. 22, pp. 2846–2856, Aug. 2012.

[36] F. Camacho, J. Cemicharo, R. Lacaze, F. Baret, and M. Weiss, "GEOV1: LAI, FAPAR essential climate variables and FCOVER global time series capitalizing over existing products. Part 2: Validation and intercomparison with reference products," *Remote Sens. Environ.*, vol. 137, pp. 310–329, Oct. 2013.

[37] W. B. Cohen, T. K. Maiersperger, Z. Q. Yang, S. T. Gower, D. P. Turner, W. D. Ritts, M. Berterretche, and S. W. Running, "Comparisons of land cover and LAI estimates derived from ETM plus and MODIS for four sites in North America: A quality assessment of 2000/2001 provisional MODIS products," *Remote Sens. Environ.*, vol. 88, no. 3, pp. 233–255, Dec. 2003.

[38] A. Di Gregorio, "Land cover classification system: Classification concepts and user manual for software–version 2," in *Food and Agriculture Organization of the United Nations, Environmental and Natural Resources Series 8*, Rome, Italy, 2005.

[39] E. F. Vermote, N. ElSaleous, C. O. Justice, Y. J. Kaufman, J. L. Privette, L. Remer, J. C. Roger, and D. Tanre, "Atmospheric correction of visible to middle-infrared EOS-MODIS data over land surfaces: Background, operational algorithm and validation," *J. Geophys. Res.*, vol. 102, no. D14, pp. 17131–17141, Jul. 1997.

[40] Y. B. Liu, W. M. Ju, G. L. Zhu, J. M. Chen, B. L. Xing, J. F. Zhu, and Y. L. Zhou, "Retrieval of leaf area index for different grasslands in Inner Mongolia prairie using remote sensing data," (in Chinese) *Acta Ecologica Sinica*, vol. 31, no. 18, pp. 5159–5170, Sep. 2011.

[41] L. Qian and Y. Song, "Analysis of relief amplitude in Liupan mountain based on DEM," (in Chinese) *J. Earth Env.*, vol. 2, no. 4, pp. 510–515, Aug. 2011.

[42] S. Plummer, J. M. Chen, G. Dedieu, and M. Simpson, GLOBCARBON Expert Support Laboratory Input and Output Definition, 1.0 ed., ESRIN, European Space Agency. GLBC/ESL/IODD, Frascati, Italy, 2002.

[43] J. M. Chen and S. G. Leblanc, "Multiple-scattering scheme useful for hyperspectral geometrical optical modelling," *IEEE Trans. Geosci. Remote Sens.*, vol. 39, no. 5, pp. 1061–1071, May 2001.
[44] L. J. Brown, J. M. Chen, S. G. Leblanc, and J. Cihlar, "Short wave infrared correction to the simple ratio: An image and model analysis," *Remote Sens. Environ.*, vol. 71, no. 1, pp. 16–25, 2000.
[45] C. J. Willmott, "On the validation of models," *Phys. Geogr.*, vol. 2, pp. 184–194, 1981.
[46] M. Huang and J. Ji, "The spatial-temporal distribution of leaf area index in China: A comparison between ecosystem modeling and remote sensing reversion," *Acta Ecologica Sinica*, vol. 30, no. 11, pp. 3057–3064, 2010.

Lin Zhu received the M.S. degree from Nankai University, Tianjin, China, in 2005 and the Ph.D. degree in Cartography and GIS from Peking University, Beijing, China. From 2007 to 2008, she was a visiting student with the University of Toronto, Toronto, ON, Canada.

She is currently an Associate Professor with the Meteorological Research Institute of the National Satellite Meteorological Center of the China Meteorological Administration. Her current research interests include the retrieval theory of land surface parameters and the related application research.

Jing M. Chen received the B.Sc. degree in applied meteorology from the Nanjing Institute of Meteorology, Nanjing, China, in 1982, and the Ph.D. degree in meteorology from Reading University, Reading, U.K., in 1986.

He was a Postdoctoral Fellow and Research Associate with the University of British Columbia, Vancouver, BC, Canada, from 1989 to 1993. From 1993 to 2000, he was a Research Scientist with the Canada Centre for Remote Sensing, Ottawa, ON, Canada. He is currently a Professor with the University of Toronto, Toronto, ON, Canada, and an Adjunct Professor with York University, Toronto. He has authored over 200 papers in refereed journals. His current research interests include the remote sensing of biophysical parameters, plant canopy radiation modeling, terrestrial water and carbon cycle modeling, and atmospheric inverse modeling for global and regional carbon budget estimation.

Dr. Chen is a Fellow of the Royal Society of Canada and a Senior Canada Research Chair. He served as an Associate Editor of the IEEE TRANSACTIONS ON GEOSCIENCE AND REMOTE SENSING from 1996 to 2002.

Shihao Tang received the M.S. degree from Nanjing Institute of Meteorology, Nanjing, China, in 1996 and the Ph.D. degree in remote sensing and GIS from Beijing Normal University.

He was a Postdoctoral associates with the Beijing Normal University, Beijing, China, from 2001 to 2003. From 2003 to 2004, he was a visiting scholar with the University of Toronto, Toronto, ON, Canada. He is currently a Professor and vice director with Meteorological research institute of National satellite meteorological center of China Meteorological Administration. His current research interests include the inversion theory of quantitative remote sensing, remote sensing product generation algorithm, and application research.

Dr. Tang is a Fellow of Satellite Meteorology Committee of China Meteorological Society and Committee of Ecological and Agricultural Meteorology.

Guicai Li received the Ph.D. degrees in Cartography and GIS from the Institute of Remote Sensing Applications, Chinese Academy of Sciences (CAS), in 2004.

He was an Assistant Professor in the National Satellite Meteorological Center (NSMC), China Meteorological Administrator (CMA) from 2004 to 2006. Since November 2006, he has been an Associate Professor in NSMC/CMA. He is an author of more than 30 articles. His research interests include the remote sensing inversion of vegetation parameters, ecosystem simulation, and carbon cycles. Dr. Li mainly worked in the algorithm developing and the product validation for satellite land surface product. He is the Chief designer of Large Experiment System (LES) of Fenyun-3 currently, in charge of the designing and the conducting of the Large Experiment System (LES), which is consisted by the aircraft experiment, Calibration and Validation. He have built the field observation system for LST validation and other products in Xilinhot, Dunhuang and other sites since 2008. Dr. Li is a member of National Technical Committee 540 on Climate and Climate Change of Standardization Administration of China (SAC/TC540). He also is a member of the Work Group for Layout Designing and Optimizing of China Meteorological Stations (LDOS-WG).

Zhaodi Guo received the B.S. degree in environmental sciences from Peking University, Beijing, China, in 2005, and the Ph.D. degree in physical geography from Peking University, Beijing, China, in 2011.

Since 2011, she has been an Assistant Research Scientist with the National Satellite Meteorological Center, Beijing, China. Her current research interests include carbon stocks estimation and carbon sinks analysis.